CHEMISTRY
A EUROPEAN JOURNAL

DOI: 10.1002/chem.201001737

VIP

Oligo-*m*-phenyleneoxalamide Copper(II) Mesocates as Electro-Switchable Ferromagnetic Metal–Organic Wires

Emilio Pardo,[a, c] Jesús Ferrando-Soria,[c] Marie-Claire Dul,[a, f] Rodrigue Lescouëzec,[a] Yves Journaux,*[a, b] Rafael Ruiz-García,[c, d] Joan Cano,[c, d] Miguel Julve,[c] Francesc Lloret,*[c] Laura Cañadillas-Delgado,[e, g, h] Jorge Pasán,[e] and Catalina Ruiz-Pérez[e]

Abstract: Double-stranded copper(II) string complexes of varying nuclearity, from di- to tetranuclear species, have been prepared by the Cu^{II}-mediated self-assembly of a novel family of linear homo- and heteropolytopic ligands that contain two outer oxamato and either zero (**1b**), one (**2b**), or two (**3b**) inner oxamidato donor groups separated by rigid 2-methyl-1,3-phenylene spacers. The X-ray crystal structures of these Cu^{II}_n complexes ($n=2$ (**1d**), 3 (**2d**), and 4 (**3d**)) show a linear array of metal atoms with an overall twisted coordination geometry for both the outer CuN_2O_2 and inner CuN_4 chromophores. Two such nonplanar *all-syn* bridging ligands **1b**–**3b** in an *anti* arrangement clamp around the metal centers with alternating *M* and *P* helical chiralities to afford an overall double *meso*-helicate-type architecture for **1d**–**3d**. Variable-temperature (2.0–300 K) magnetic susceptibility and variable-field (0–5.0 T) magnetization measurements for **1d**–**3d** show the occurrence of $S=nS_{Cu}$ ($n=2$–4) high-spin ground states that arise from the moderate ferromagnetic coupling between the unpaired electrons of the linearly disposed Cu^{II} ions ($S_{Cu}={}^1/_2$) through the two *anti* *m*-phenylenediamidate-type bridges (*J* values in the range of $+15.0$ to $16.8\ cm^{-1}$). Density functional theory (DFT) calculations for **1d**–**3d** evidence a sign alternation of the spin density in the *meta*-substituted phenylene spacers in agreement with a spin polarization exchange mechanism along the linear metal array with overall intermetallic distances between terminal metal centers in the range of 0.7–2.2 nm. Cyclic voltammetry (CV) and rotating-disk electrode (RDE) electrochemical measurements for **1d**–**3d** show several reversible or quasireversible one- or two-electron steps that involve the consecutive metal-centered oxidation of the inner and outer Cu^{II} ions ($S_{Cu}={}^1/_2$) to diamagnetic Cu^{III} ones ($S_{Cu}=0$) at relatively low formal potentials (*E* values in the range of $+0.14$ to 0.25 V and of $+0.43$ to 0.67 V vs. SCE, respectively). Further developments may be envisaged for this family of oligo-*m*-phenyleneoxalamide copper(II) double mesocates as electro-switchable ferromagnetic 'metal–organic wires' (MOWs) on the basis of their unique ferromagnetic and multicenter redox behaviors.

Keywords: copper · density functional calculations · magnetic properties · mesocates · redox properties

[a] Dr. E. Pardo, Dr. M.-C. Dul, Dr. R. Lescouëzec, Dr. Y. Journaux
Institut Parisien de Chimie Moléculaire
UPMC Univ Paris 06, Paris, 75252 (France)
Fax: (+33) 144273841
E-mail: jour@ccr.jussieu.fr

[b] Dr. Y. Journaux
CNRS, UMR 7201, Paris, 75005 (France)

[c] Dr. E. Pardo, J. Ferrando-Soria, Dr. R. Ruiz-García, Dr. J. Cano, Prof. Dr. M. Julve, Prof. Dr. F. Lloret
Departament de Química Inorgànica/
Instituto de Ciencia Molecular (ICMol)
Universitat de València, Paterna, Valencia, 46980 (Spain)
Fax: (+34) 963-544-322
E-mail: francisco.lloret@uv.es

[d] Dr. R. Ruiz-García, Dr. J. Cano
Fundació General de la Universitat de València (FGUV)
Universitat de València, Valencia, 46002 (Spain)

[e] Dr. L. Cañadillas-Delgado, Dr. J. Pasán, Prof. Dr. C. Ruiz-Pérez
Laboratorio de Rayos X y Materiales Moleculares
Departamento de Física Fundamental II, Facultad de Física
Universidad de la Laguna, La Laguna, Tenerife, 38201 (Spain)

[f] Dr. M.-C. Dul
Department of Chemistry, Memorial University
St. John's, Newfoundland, A1B 3X7 (Canada)

[g] Dr. L. Cañadillas-Delgado
Instituto de Ciencia de Materiales de Aragón
CSIC-Universidad de Zaragoza, Zaragoza, 50009 (Spain)

[h] Dr. L. Cañadillas-Delgado
Institut Laue Langevin, Grenoble, 38042 (France)

Supporting information for this article is available on the WWW under http://dx.doi.org/10.1002/chem.201001737.

Introduction

Supramolecular coordination chemistry has been an outstanding area of research in the field of supramolecular chemistry,[1] which has set up the guiding principles for the self-assembly of well-defined multimetallic coordination architectures of increasing structural complexity based on metal–ligand interactions.[2] The focus of the current research in supramolecular coordination chemistry (so-called metallosupramolecular chemistry) moves toward the introduction of functionality into these polymetallic systems.[3–9] The main reason for the interest in these nanosized, self-assembling functional metallosupramolecular complexes is the very unusual electronic (magnetic and redox) properties that they can exhibit, which could be exploited in the related fields of molecular magnetism and electronics.[10]

Linear multiple-stranded polynuclear helicates and related *meso*-helicates, so-called mesocates, were the object of much attention as model systems for the study of metal-directed self-assembling processes.[11] Since the seminal research on double-stranded di- and trinuclear helicates with oligobipyridine ligands and tetrahedral Cu^{I} ions by Lehn et al.,[12] much work has been devoted to the search for the structure and function of helicates and mesocates.[13,14] Although their redox behavior has attracted great interest,[13] it was not until recently that several groups have focused on the magnetic properties of helicates and mesocates.[14] Besides their actual interest as models for the fundamental research on electron-exchange (EE) and electron-transfer (ET) phenomena, homo- and heterovalent exchange-coupled helicates and mesocates will be of great importance in the "bottom-up" approach to molecular-level spintronic devices. Molecular wires and molecular switches are two representative examples of the potential applications of such a class of ligand-supported, linear metallosupramolecular complexes in information storage and processing nanotechnology.[15]

Ligand design is crucial in the pursuit of functional helicates and mesocates, both to organize the paramagnetic metal ions in the desired linear topology and to efficiently transmit the electronic interactions between the metal ions—either directly, through metal–metal bonds, or indirectly, through the organic bridging ligands. This basic principle is illustrated by the impressive work carried out by the groups of Cotton and Peng on the redox and magnetic properties of self-assembled transition-metal complexes of varying nuclearities that extend from tri- to nonanuclear species, with linear oligo-α-pyridylamine and related pyrazine-, pyrimidine-, and naphthyridine-modified ligands.[16–21] This series of moderately strong, antiferromagnetically coupled quadruple mesocates with a string of three to nine shortly spaced M^{II} ions (M = Cu, Ni, Co, Cr, Pd, Pt, Ru, and Rh) have attracted considerable attention for fundamental research on the effect of metal–metal bonding interactions on ET properties, because they will probably allow them to function as molecular electronic wires and switches.[15]

Similar studies on the EE properties between distant metal centers through extended organic bridges in oligonuclear transition-metal helicates and mesocates beyond dinuclear species are relatively scarce.[22] For example, a tetracopper(II) triple helicate with a bis(α-pyridylazine)pyridazine ligand and a hexacopper(II) double helicate with an oligo-α-pyridylcarboxamido ligand have been reported by the groups of Matthews and Huc, respectively.[22] However, the magnetic behavior (whenever reported) of these oligonuclear helicates with a string of four and six Cu^{II} ions is that of the isolated spins, with negligible or very weak antiferromagnetic interactions between the metal centers through the organic bridging ligands.[22a]

In our research on ligand design as a means to control the molecular and electronic structure of oxalamide-based transition-metal complexes,[23–25] we report a new double-stranded dicopper(II) complex of the *meso*-helicate-type that results from the side-by-side self-assembly of two *N,N′*-1,3-phenylenebis(oxamate) bridging ligands by two Cu^{II} ions.[25a]

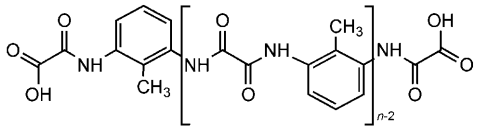

$H_{2n}\mathbf{L}$
($n = 2$–4)

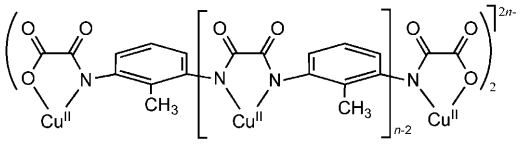

$[Cu_n\mathbf{L}_2]^{2n-}$
($n = 2$–4)

Notably, this dinuclear double mesocate is among the first transition-metal complexes for which the ferromagnetic coupling between the two metal ions is due to spin polarization effects that arise from the alternation of the spin density at the double *meta*-phenylenediamidate bridge within the resulting metallacyclophane core, as evidenced by density functional theory (DFT) calculations.[25a] Through a sequential addition of oxamidato binding sites to this parent homotopic dioxamato ligand, it would be possible to prepare higher-nuclearity copper(II) analogues with a linear topology that exhibit ferromagnetic coupling between the metal centers as well as metal-centered redox activity because of the well-known strong donor ability (basicity) of the oxamidato donor groups.[23a,d,e] They therefore constitute a new class of molecular magnetic wires and switches for the transmission of 'through-bond' metal–metal EE interactions, by analogy with the aforementioned molecular electronic wires and switches that were based on direct 'through-space' metal–metal ET interactions.[25b–d] In contrast to conventional molecular electronic wires and switches, these molecular

magnetic wires and switches may offer a new design concept for the transfer of information over long distances based on purely EE (Coulomb) interactions and with no current flow.

We report here the syntheses, crystal structures, redox, and magnetic properties of this novel series of double-stranded copper(II) complexes of the general formula $[Cu^{II}_{n}\mathbf{L}_2]^{2n-}$ ($n=2$–4), in which **L** is the 2-methyl-substituted derivative of the *N,N′*-1,3-phenylenebis(oxamate) ligand (**L**=**1b**) and its corresponding longer heterotopic analogues with one (**L**=**2b**) and two (**L**=**3b**) additional oxamidato binding sites, respectively. DFT calculations on this unique family of oligonuclear double mesocates with linear oligo-*m*-phenyleneoxalamide ligands, which extends from di- to tetranuclear species, were also performed to support the occurrence of a spin polarization mechanism for the propagation of an EE interaction of a ferromagnetic nature between the metal centers through the methyl-substituted *meta*-phenylene spacers.

Results and Discussion

Syntheses of the ligands and complexes: The ligands were synthesized from the straightforward condensation of the corresponding diamine precursors H_{2n-4}**1a**–H_{2n-4}**3a** ($n=2$–4) with ethyl oxalyl chloride ester (1:2 ratio) in tetrahydrofuran in the presence of triethylamine, and they were isolated as the diethyl ester acid derivatives $H_{2n-2}Et_2$**L** (**L**=**1b**–**3b**; $n=$ 2–4) in pure form and very good yields (90–97%) (Scheme 1a, c, and e). The parent 2-methyl-1,3-phenylenediamine (**1a**) was commercially available, whereas the two other diamine precursors, namely, *N,N′*-bis(2-methyl-3-phenylamine)oxamide (H_2**2a**) and 2-methyl-1,3-phenylenebis-[*N′*-(2-methyl-3-phenylamine)oxamide] (H_4**3a**), were in turn prepared from the reaction of the diethyl ester derivative of either oxalic acid or *N,N′*-2-methyl-1,3-phenylenebis(oxamic acid) (H_2Et_2**1b**) with an excess amount of fused 2-methyl-1,3-phenylenediamine (1:10 ratio) in moderate to good yields (67–72%) (Scheme 1b and d, respectively).

The anionic oligonuclear copper(II) complexes $[Cu_n\mathbf{L}_2]^{2n-}$ ($n=2$–4) were isolated as either the alkaline or tetra(aryl/alkyl) ammonium and phosphonium salts of formula $Na_4[Cu_2(\mathbf{1b})_2]\cdot 6H_2O$ (**1c**), $Na_6[Cu_3(\mathbf{2b})_2]\cdot 20H_2O$ (**2c**), $Na_8[Cu_4(\mathbf{3b})_2]\cdot 16H_2O$ (**3c**), $(n\mathrm{Bu}_4\mathrm{N})_4[Cu_2(\mathbf{1b})_2]\cdot 4H_2O$ (**1d**), $(EtPh_3P)_6[Cu_3(\mathbf{2b})_2]\cdot 26.7H_2O$ (**2d**), and $(EtPh_3P)_8[Cu_4(\mathbf{3b})_2]\cdot 16H_2O$ (**3d**) in good yields (85–95%). Complexes **1c**–**3c** were prepared by the one-step reaction of the corresponding proligand $H_{2n-2}Et_2$**L** (**L**=**1b**–**3b**; $n=2$–4) with copper(II) nitrate in the appropriate 2:*n* molar ratio by using either sodium(I) hydroxide or hydride as base in water or dimethylformamide, respectively (Scheme 2a and b). The former method was employed for the shorter ligands (**L**=**1b** and **2b**) with rather good results, whereas the latter method was used for the longest one (**L**=**3b**) because of ligand insolubility and/or deprotonation problems. Complex **1d** was similarly synthesized by the one-step reaction of the corresponding proligand H_2Et_2**1b** with copper(II) chloride in the appropriate 2:2 molar ratio by using tetra-*n*-butylammonium hydroxide as base in water followed by extraction with dichloromethane (Scheme 2c). Alternatively, complexes **2d** and **3d** were synthesized by two successive steps after metathesis of the corresponding sodium(I) salts **2c** and **3c** with ethyltriphenylphosphonium bromide in water/acetonitrile through the intermediacy of the silver(I) salts (Scheme 2d and e). The inorganic salts (**1c**–**3c**) were soluble in water, whereas the organic ones (**1d**–**3d**) were sparingly soluble in organic solvents like acetonitrile.

The chemical identity of the ligands and complexes was established by elemental analysis and ^{1}H NMR, FTIR, and UV/Vis spectroscopies (see the Experimental Section). The structures of **1d**–**3d** were further confirmed by single-crystal X-ray diffraction using the synchrotron radiation. A summary of the crystallographic data for **1d**–**3d** is given in Table 1.

Description of the structures: The structures of **1d**–**3d** consist of double-stranded di-, tri-, and tetranuclear copper(II) anions, $[Cu^{II}_2(\mu_2\text{-}\kappa^2\text{:}\kappa^2\text{-}\mathbf{1b})_2]^{4-}$, $[Cu^{II}_3(\mu_3\text{-}\kappa^2\text{:}\kappa^2\text{:}\kappa^2\text{-}\mathbf{2b})_2]^{6-}$, and $[Cu^{II}_4(\mu_4\text{-}\kappa^2\text{:}\kappa^2\text{:}\kappa^2\text{:}\kappa^2\text{-}\mathbf{3b})_2]^{8-}$, respectively (Figures 1–3), tetra-

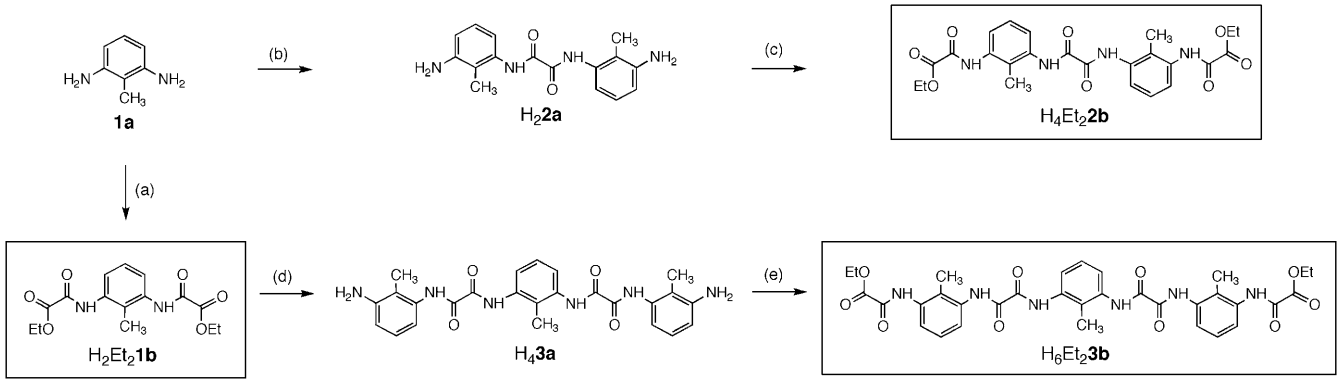

Scheme 1. Synthetic procedure for the diethyl ester acid derivatives of the oligo-*m*-phenylene oxalamide ligands $H_{2n-2}Et_2$**L** (**L**=**1b**–**3b**; $n=2$–4) from the corresponding diamine precursors H_{2n-4}**1a**–**3a**. Reaction conditions: a) $C_2O_2Cl(OEt)$, Et_3N, THF (80°C); b) $C_2O_2(OEt)_2$ (120°C); c) $C_2O_2Cl(OEt)$, Et_3N, THF (80°C); d) 2-Me-1,3-$C_6H_4NH_2$ (120°C); and e) $C_2O_2Cl(OEt)$, Et_3N, THF (80°C).

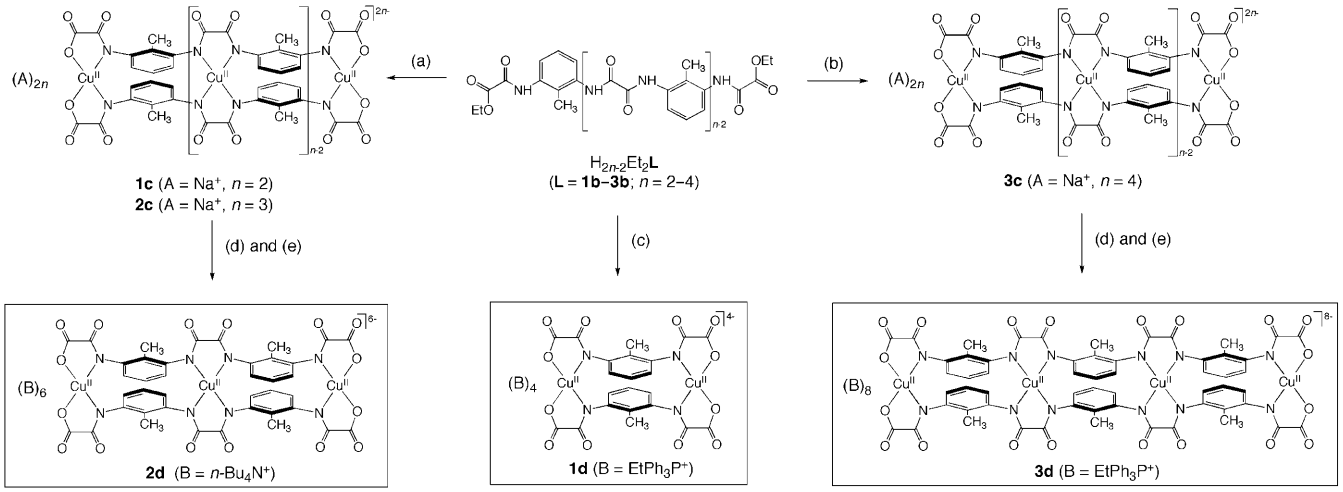

Scheme 2. Synthetic procedure for the tetra(alkyl/aryl) ammonium and phosphonium salts of the anionic oligo-*m*-phenylene oxalamide copper(II) complexes $[Cu_nL_2]^{2n-}$ (**L**=**1b**–**3b**; n=2–4) from the corresponding sodium salts. Reaction conditions: a) NaOH, $Cu(NO_3)_2$, H_2O (RT); b) NaH, $Cu(NO_3)_2$, DMF (RT); c) nBu_4NOH, $CuCl_2$, H_2O/CH_2Cl_2 (RT); d) $AgNO_3$, H_2O (RT); and e) $EtPh_3PBr$, H_2O/CH_3CN (RT).

Table 1. Summary of crystallographic data for **1d**–**3d**.

	1d	**2d**	**3d**
formula	$C_{86}H_{164}Cu_2N_8O_{16}$	$C_{160}H_{197.4}Cu_3N_8O_{42.7}P_6$	$C_{218}H_{228}Cu_4N_{12}O_{36}P_8$
M_r [g mol^{-1}]	1693.27	3292.67	4094.17
crystal system	monoclinic	orthorhombic	triclinic
space group	*C*2/*c*	*Pbcn*	$P\bar{1}$
a [Å]	23.959(5)	24.9780(10)	18.140(4)
b [Å]	19.353(4)	21.9780(10)	18.340(4)
c [Å]	22.494(5)	31.6890(10)	19.150(4)
α [°]	90.0	90.0	117.86(3)
β [°]	115.59(3)	90.0	107.74(3)
γ [°]	90.0	90.0	90.84(3)
V [Å^3]	9407(3)	17396.2(12)	5271(2)
Z	4	4	1
ρ_{calcd} [g cm^{-3}]	1.190	1.237	1.287
μ [mm^{-1}]	0.515	0.494	0.531
T [K]	100(2)	100(2)	100(2)
independent reflns	10151	9454	16440
obsd reflns [$I>2\sigma(I)$]	8527	8845	13161
R[a] ($I>2\sigma(I)$)	0.0928	0.0785	0.0856
wR[b] ($I>2\sigma(I)$)	0.2334	0.2308	0.2653
GOF[c]	1.066	1.048	1.027

[a] $R=\Sigma(|F_o|-|F_c|)/\Sigma|F_o|$. [b] $wR=[\Sigma w(|F_o|-|F_c|)^2/\Sigma w|F_o|^2]^{1/2}$. [c] GOF = $[\Sigma w(|F_o|-|F_c|)^2/(N_o-N_p)]^{1/2}$.

n-butylammonium or ethyltriphenylphosphonium cations, and crystallization water molecules. The di- and tetracopper(II) anions of **1d** and **3d** are centrosymmetric, whereas the tricopper(II) anions of **2d** have a crystallographically imposed twofold symmetry. A summary of the structural data for **1d**–**3d** is given in Table 2. Selected bond lengths and interbond angles for **1d**–**3d** are listed in Tables 3–5.

Each pseudo C_h-(**1b** and **3b**) or C_2-symmetric (**2b**) bridging ligand in **1d**–**3d** possesses a nonplanar, almost orthogo-

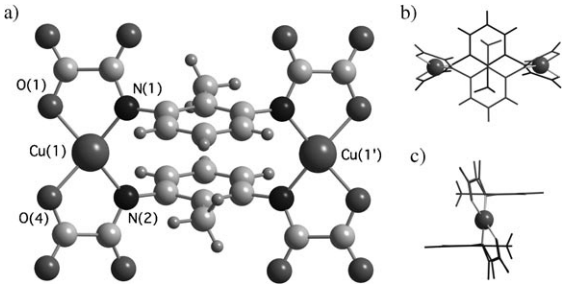

Figure 1. a) Perspective view of the anionic dicopper(II) unit of **1d** with the atom-numbering scheme for the metal environments (symmetry code: (I) = $-x$, $-y$, $1-z$). b) Top and c) side views of the dicopper(II) double mesocate of **1d** showing each ligand strand with a different tonality.

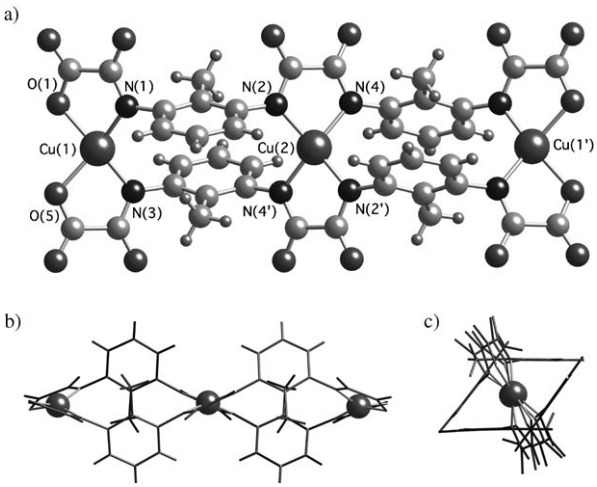

Figure 2. a) Perspective view of the anionic tricopper(II) unit of **2d** with the atom-numbering scheme for the metal environments (symmetry code: (I) = $-x$, y, $^1/_2-z$). b) Top and c) side views of the tricopper(II) double mesocate of **2d** showing each ligand strand with a different tonality.

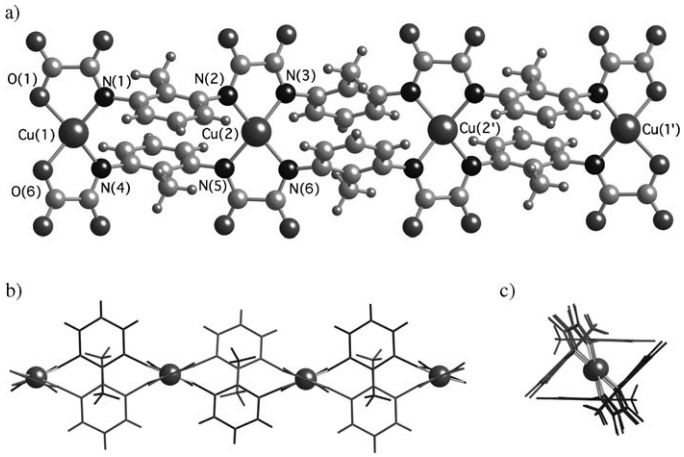

Figure 3. a) Perspective view of the anionic tetracopper(II) unit of **3d** with the atom-numbering scheme for the metal environments (symmetry code: (I) = $-x$, $1-y$, $-z$). b) Top and c) side views of the tetracopper(II) double mesocate of **3d** showing each ligand strand with a different tonality.

Table 2. Summary of structural data for **1d**–**3d**.

	1d	**2d**	**3d**
ψ[a] [°]	73.5(3)	62.1(3)	65.0(2)
	82.4(3)	84.0(4)	82.3(4)
h[b] [Å]	4.442(1)	4.168(3)	3.776(3)
			4.317(3)
ϕ[c] [°]	42.33(9)	34.7(4)	29.3(4)
			41.7(4)
α[d] [°]	126.5(2)	123.1(3)	125.5(3)
	127.0(2)	125.6(4)	126.7(4)
ϕ[e] [°]	103.4(4)	100.7(6)	105.5(5)
			112.4(6)
	105.9(4)	117.8(5)	117.2(5)
			121.5(5)
τ[f] [°]	36.55(14)	39.3(2)	38.7(2)
		43.6(2)	41.2(2)

[a] Dihedral angle between the oxalamide and the benzene planes. [b] Centroid–centroid distance between the benzene planes. [c] Offset angle between the centroid–centroid vector and the normal to the benzene plane. [d] Interbond Cu-N-C angle. [e] Torsion Cu-N-C-C angle. [f] Twist angle at the metal atoms.

nal *all-syn* conformation of the oxamato and/or oxamidato donor groups with respect to the 2-methyl-1,3-phenylene spacers. The values of the dihedral angle (ψ) between the oxalamide and the benzene planes are in the range of 73.5(3)–82.4(3) (**1d**), 62.1(3)–84.0(4) (**2d**), and 65.0(2)–82.3(4)° (**3d**) (Table 2). Two such linear bis- (**1b**), tris- (**2b**), and tetrakis(bidentate) (**3b**) ligands clamp around the two, three, and four copper atoms of **1d**–**3d** in a side-by-side *anti* arrangement. This side-by-side coordination binding mode gives rise to an overall *meso*-helicate-type structure for the anionic di-, tri, and tetracopper(II) units with approximate C_{2i} (**1d**), D_2 (**2d**), and C_{2h} (**3d**) molecular symmetries, respectively (Figure 1a, Figure 2a, and Figure 3a). More likely, the *anti* configuration of the oligonuclear copper(II) double mesocates in **1d**–**3d** obeys the steric requirements of the 2-methyl substituents, which precludes the occurrence of appreciable π–π interactions between the two parallel-displaced benzene rings within the resulting metallacyclophane cores (Figure 1b, Figure 2b, Figure 3b, and Figure 1c, Figure 2c, Figure 3c). The values of the centroid–centroid distance (h) are 4.442(1) (**1d**), 4.168(3) (**2d**), 3.776(3), and 4.317(3) Å (**3d**), and those of the offset angle (ϕ) between the centroid–centroid vector and the normal to the plane of the benzene ring are 42.33(9) (**1d**), 34.7(4) (**2d**), 29.3(4). and 41.7(4)° (**3d**) (Table 2). This situation contrasts with that found in the previously reported dicopper(II) complex with the parent unsubstituted bridging ligand *N,N'*-1,3-phenylenebis(oxamate), in which the two facing benzene rings are disposed in an eclipsed *syn* configuration so as to maximize the π–π interactions within the resulting metallacyclophane core (h = 3.3773(5) Å and ϕ = 5.36(8)°).[25a]

Within the binuclear metallacyclophane cores of **1d**–**3d**, $Cu_2(\mu\text{-}N_2C_6H_3Me)_2$, the values of the Cu-N-C angle (α) are in the range of 126.5(2)–127.0(2) (**1d**), 123.1(3)–125.6(4) (**2d**), and 125.5(3)–126.7(4)° (**3d**) (Table 2), which are similar to those reported for the related *syn* dicopper(II) double mesocate (α = 126.9(4)–132.1(4)°).[25a] These values remain close to that expected for trigonal sp^2 (α = 120.0°) rather than tetrahedral sp^3 hybridization (α = 109.4°) for the amidate nitrogen atoms. The values of the torsion angle (ϕ) around the Cu-N-C-C bonds are in the range of 103.4(4)–105.9(4) (**1d**), 100.7(6)–117.8(5) (**2d**), and 105.5(5)–121.5(5)° (**3d**) (Table 2), which are farther from 90° than those reported for the related *syn* dicopper(II) double mesocate (ϕ = 73.6(2)–97.9(2)°).[25a] Moreover, they deviate appreciably more from 90° for the central metallacyclophane core (ϕ = 117.2(5)–121.5(5)°) than for the two peripheral ones (ϕ = 105.5(6)–112.4(6)°) in **3d** (Table 2), thereby reflecting a larger distortion from orthogonality between the mean metal basal planes and the benzene rings.

Both the outer Cu(1) and inner Cu(2) atoms in **1d**–**3d** adopt a unique four-coordinated twisted geometry, which is built by either two amidate nitrogen and two carboxylate oxygen atoms from two bidentate oxamato donor groups, $Cu(1)N_2O_2$, or by four amidate nitrogen atoms from two bidentate oxamidato donor groups, $Cu(2)N_4$, respectively. Thus, the values of the twist angle (τ) of 36.55(14)° for the Cu(1) atom in **1d** (Table 2) are intermediate between those expected for square planar (τ = 0°) and tetrahedral (τ = 90°) geometries, in contrast with the related *syn* dicopper(II) double mesocate, which possesses a geometry close to square planar (τ = 12.3(2)°).[25a] The τ values of 43.6(2) (**2d**) and 41.2(2)° (**3d**) for the Cu(2) atom are even greater than those of 39.3(2) (**2d**) and 38.7(2)° (**3d**) for the Cu(1) atom (Table 2), thus indicating a stronger tetrahedral distortion for the inner metal coordination site than for the outer one in **2d** and **3d**, most likely because of the steric requirements of the rigid mesocate structure. The values of the Cu(1)–N(amidate) bond lengths in the range of 1.925(3)–1.944(3) (**1d**), 1.947(5)–1.965(6) (**2d**), and 1.938(5)–1.943(5) Å (**3d**) are shorter than those of the Cu(1)–O(carboxylate) ones, which are in the range of 1.946(3)–1.961(3) (**1d**), 2.035(6)–

2.065(5) (**2d**), and 1.952(4)–1.956(5) Å (**3d**) (Table 3, Table 4, and Table 5), as previously found in the related *syn* dicopper(II) double mesocate (Cu–N = 1.925(5)–1.969(5) Å and Cu–O = 1.928(4)–1.995(4) Å).[25a] This is as expected from the well-known stronger ligand field of the amidate nitrogen donor atoms compared to the carboxylate oxygen ones.[23a] The values of the Cu(2)–N(amidate) bond lengths in the range of 1.960(4)–1.986(4) (**2d**) and 1.965(4)–1.973(4) Å (**3d**) (Tables 4 and 5) are, however, slightly longer than those of the Cu(1)–N(amidate) ones, likely reflecting the stronger tetrahedral distortion of the inner copper atoms compared to the outer ones.

Table 3. Selected bond lengths [Å] and interbond angles [°] for **1d**.[a]

Cu(1)–N(1)	1.944(3)	Cu(1)–N(2)	1.925(3)
Cu(1)–O(1)	1.946(3)	Cu(1)–O(4)	1.961(3)
N(1)-Cu(1)-N(2)	107.58(13)	N(1)-Cu(1)-O(1)	84.29(14)
N(1)-Cu(1)-O(4)	149.64(15)	N(2)-Cu(1)-O(1)	153.0(2)
N(2)-Cu(1)-O(4)	84.18(12)	O(1)-Cu(1)-O(4)	97.69(13)

[a] The estimated standard deviations are given in parentheses.

Table 4. Selected bond lengths [Å] and interbond angles [°] for **2d**.[a,b]

Cu(1)–N(1)	1.965(6)	Cu(1)–N(3)	1.947(5)
Cu(1)–O(1)	2.035(6)	Cu(1)–O(5)	2.065(5)
Cu(2)–N(2)	1.960(4)	Cu(2)–N(4)	1.986(4)
N(1)-Cu(1)-N(3)	110.0(2)	N(1)-Cu(1)-O(1)	82.6(2)
N(1)-Cu(1)-O(5)	151.2(2)	N(3)-Cu(1)-O(1)	155.8(2)
N(3)-Cu(1)-O(5)	82.3(2)	O(1)-Cu(1)-O(5)	96.5(2)
N(2)-Cu(2)-N(4)	103.85(18)	N(2)-Cu(2)-N(2^{I})	153.2(3)
N(2)-Cu(2)-N(4^{I})	83.18(18)	N(4)-Cu(2)-N(4^{I})	149.8(3)

[a] The estimated standard deviations are given in parentheses. [b] Symmetry code: (I) = $-x$, y, $^{1}/_{2}-z$.

Table 5. Selected bond lengths [Å] and interbond angles [°] for **3d**.[a]

Cu(1)–N(1)	1.938(5)	Cu(1)–N(4)	1.943(5)
Cu(1)–O(1)	1.956(5)	Cu(1)–O(6)	1.952(4)
Cu(2)–N(2)	1.967(4)	Cu(2)–N(3)	1.965(4)
Cu(2)–N(5)	1.973(4)	Cu(2)–N(6)	1.965(4)
N(1)-Cu(1)-N(4)	106.47(19)	N(1)-Cu(1)-O(1)	84.1(2)
N(1)-Cu(1)-O(6)	152.2(2)	N(4)-Cu(1)-O(1)	155.5(2)
N(4)-Cu(1)-O(6)	84.06(18)	O(1)-Cu(1)-O(6)	96.8(2)
N(2)-Cu(2)-N(3)	82.58(17)	N(2)-Cu(2)-N(5)	104.67(17)
N(2)-Cu(2)-N(6)	153.85(19)	N(3)-Cu(2)-N(5)	152.29(18)
N(3)-Cu(2)-N(6)	102.79(16)	N(5)-Cu(2)-N(6)	82.58(17)

[a] The estimated standard deviations are given in parentheses.

The two centrosymmetrically related Cu(1) and Cu(1^{I}) atoms in **1d** possess alternating helical chiralities (*M*,*P* configuration), thus leading to an overall achiral dicopper(II) double mesocate. Alternatively, there exists a racemic mixture of tricopper(II) double mesocates in **2d** with alternating *M*,*P*,*M* and *P*,*M*,*P* helical chiralities at the twofold symmetrically related Cu(1) and Cu(1^{I}) atoms and the Cu(2) atom, which are almost collinear (Cu(1)-Cu(2)-Cu(1^{I}) = 177.53(1)°). The two pairs of almost collinear, centrosymmetrically related Cu(1)/Cu(1^{I}) and Cu(2)/Cu(2^{I}) atoms in **3d** (Cu(1)-Cu(2)-Cu(2^{I}) = 176.91(2)°) also have alternating helical chiralities, thus leading to an overall achiral double mesocate (*M*,*P*,*M*,*P* configuration), as in **1d**. This series of heterochiral double mesocates contrasts with the more abundant homochiral double helicates reported in the literature, which result instead from helical wrapping of the ligands around the metal centers.[12] The values of the intermetallic distance (*r*) between adjacent copper atoms across the two 2-methyl-substituted 1,3-phenylenediamidate bridges in an *anti* conformation for **1d**–**3d** are comparable (Cu(1)–Cu(1^{I}) = 7.2019(12) Å (**1d**), Cu(1)–Cu(2) = 7.3536(10) Å (**2d**), Cu(1)–Cu(2) = 7.294(2) Å, and Cu(2)–Cu(2^{I}) = 7.395(2) Å (**3d**)), which are somewhat greater than that of the related *syn* dicopper(II) double mesocate (*r* = 6.822(2) Å).[25a] Otherwise, the values of the intermetallic distance between the terminal copper atoms for **1d**–**3d** increase progressively along this series of *anti* oligocopper(II) double mesocates (Cu(1)–Cu(1^{I}) = 7.2019(12) (**1d**), 14.7037(15) (**2d**), and 21.975(5) Å (**3d**)).

In the crystal lattice of **1d**–**3d**, the anionic oligonuclear copper(II) units establish diverse hydrogen bonds with the crystallization water molecules through the carbonyl and/or carboxylate oxygen atoms from the oxamato and/or oxamidato groups (O···Ow = 2.762(5)–2.819(7) (**1d**), 2.701(5)–2.881(6) Å (**2d**), and 2.714(15)–2.868(11) Å (**3d**)) (Figures S1–S3 in the Supporting Information). Discrete dicopper(II) anions are aligned along the *c* axis in **1d** (Figure S1 a), which are well separated from each other by the bulky tetra-*n*-butylammonium cations (Figure S1 b). In contrast, the tri- and tetracopper(II) anions of **2d** and **3d**, respectively, are connected with each other through a variety of hydrogen bonds that involve the hydrogen-bonded crystallization water molecules (Ow···Ow = 2.64(2)–2.91(2) (**2d**) and 2.730(18)–2.894(12) Å (**3d**)). This situation gives rise to either extended layers of hydrogen-bonded tricopper(II) anions that grow in the *ac* plane for **2d** (Figure S2 a) or chains of hydrogen-bonded tetracopper(II) anions along the [101] direction for **3d** (Figure S3 a), which are well separated from each other by the bulky ethyltriphenylphosphonium cations (Figure S2 b and S3 b). The value of the shortest intermolecular Cu(1)–Cu(1^{II}) distance in **1d** is 8.184(2) Å, whereas those of the shortest intermolecular Cu(1)–Cu(1^{II}) and Cu(1)–Cu(2^{II}) distances across the hydrogen-bonded crystallization water molecules in **2d** and **3d** are 11.3909(15) and 16.672(7) Å, respectively (Figures S1 a–S3 a).

Redox properties: The cyclic voltammograms of **1d**–**3d** in acetonitrile (25 °C, 0.1 M nBu$_4$NPF$_6$) are shown in Figure 4. A summary of the electrochemical data for **1d**–**3d** is given in Table 6.

Complex **1d** shows two closely spaced, quasireversible one-electron oxidation waves at formal potentials of E_1 = +0.43 V and E_2 = +0.65 V versus SCE, with anodic to cathodic peak separation values of ΔE_1 = 80 mV and ΔE_2 = 100 mV, respectively (solid line in Figure 4a). Complex **2d** shows a reversible one-electron oxidation wave at a much lower formal potential value of E_1 = +0.17 V versus SCE

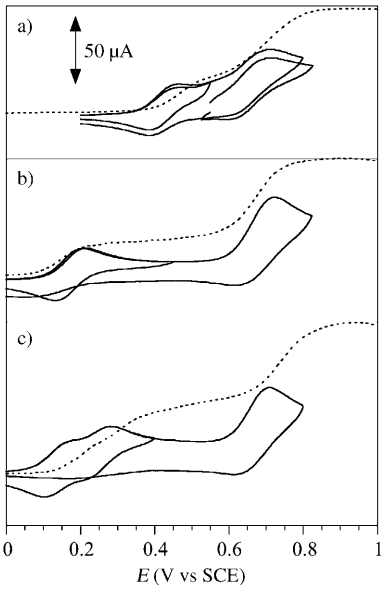

Figure 4. CV and RDE voltammograms (solid and dotted lines, respectively) of a) **1d**, b) **2d**, and c) **3d** in acetonitrile (25 °C, 0.1 M nBu$_4$NPF$_6$).

Table 6. Selected electrochemical data for **1d**–**3d**.[a]

Complex	E_1[b] [V]	E_2[b] [V]	E_3[b] [V]	ΔE_{12}[c] [mV]	K_c[d]
1d	+0.43 (80)	+0.65 (100)		220	0.5×10^4
2d	+0.17 (70)	+0.67 (90)			
3d	+0.14 (70)	+0.25 (70)	+0.66 (90)	110	0.7×10^2

[a] In acetonitrile (25 °C, 0.1 M nBu$_4$NPF$_6$). [b] All formal potential values were taken as the half-wave potentials versus SCE. The peak-to-peak separations (ΔE) between the anodic (E_a) and cathodic (E_c) peak potentials are given in parentheses [mV]. [c] Difference in the formal potential values between the two first one-electron oxidation waves. [d] The comproportionation constant values were calculated through the expression $\log K_c = \Delta E_{12}/59$.

according to a metal-centered redox model that involves the oxidation of the paramagnetic d^9 Cu^{II} ions ($S_{Cu}=1/2$) to the diamagnetic low-spin d^8 Cu^{III} ions ($S_{Cu}=0$) (Scheme 3). Thus, the two quasireversible, one-electron redox processes for **1d** correspond to the stepwise oxidation of the two outer Cu^{II} ions to give the mixed-valent Cu^{II}Cu^{III} and the high-valent Cu$^{III}{}_2$ species, respectively (Scheme 3a). Alternatively, the first reversible, one-electron redox process of **2d** is ascribed to the oxidation of the inner Cu^{II} ion to give the stable (on the voltammetric timescale), singly oxidized mixed-valent Cu$^{II}{}_2$Cu^{III} species (Scheme 3b), whereas the two first reversible, one-electron redox processes of **3d** are accordingly ascribed to the stepwise oxidation of the two inner Cu^{II} ions to give the stable, singly- and doubly-oxidized mixed-valent species Cu$^{II}{}_3$Cu^{III} and Cu$^{II}{}_2$Cu$^{III}{}_2$, respectively (Scheme 3c). The second and the third quasireversible, two-electron redox processes of **2d** and **3d** are then assigned to the simultaneous oxidation of the two noninteracting outer Cu^{II} ions to render the triply oxidized high-valent Cu$^{III}{}_3$ and the quadruply oxidized high-valent Cu$^{III}{}_4$ species, respectively (Scheme 3b and c).

The separation in the formal potential values between the two first one-electron oxidation waves ($\Delta E_{12}=E_2-E_1$) of 220 (**1d**) and 110 mV (**3d**) is related to the ability of the 2-methyl-substituted 1,3-phenylene spacers to transmit electronic interactions between the metal centers. The observed difference in the ΔE_{12} values for **1d** and **3d** gives an estimation of the relative magnitude of the outer–outer and inner–inner pairwise electronic interactions in the corresponding mixed-valent Cu^{II}Cu^{III} and Cu$^{II}{}_3$Cu^{III} intermediates, respectively. Thus, the calculated values of the comproportionation constant (K_c) of 5000 (**1d**) and 70 (**3d**) clearly evidence the lower thermodynamic stability of the mixed-valent Cu$^{II}{}_3$Cu^{III} intermediate compared with the Cu^{II}Cu^{III} one (Table 6). The relatively weaker electronic coupling between the inner metal centers in the mixed-valent Cu$^{II}{}_3$Cu^{III} intermediate can be attributed, at least in part, to the steric hindrance of the rigid tetranuclear mesocate structure in **3d** that prevents the orthogonality between the bis(oxamidato)metal moieties and the methyl-substituted *meta*-phenylene spacers (ϕ= 119.3(5)°) (Table 2).

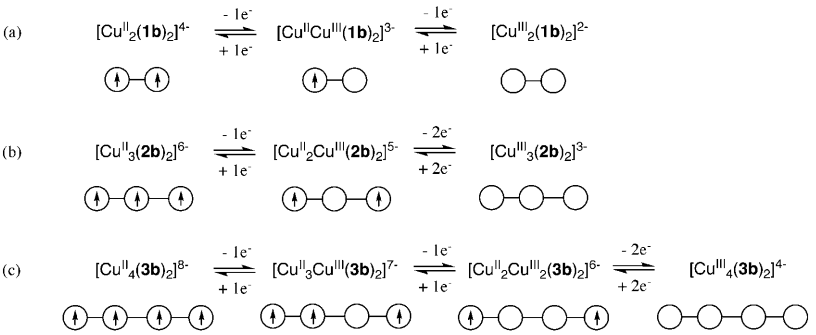

Scheme 3. Metal-centered redox model for a) **1d**, b) **2d**, and c) **3d**.

($\Delta E_1=70$ mV), which is well separated from a pseudoreversible two-electron oxidation wave at $E_2=+0.67$ V versus SCE ($\Delta E_2=90$ mV) (solid line in Figure 4b). Complex **3d** shows instead not one but two closely spaced reversible one-electron oxidation waves at low formal potential values of $E_1=+0.14$ V ($\Delta E_1=70$ mV) and $E_2=+0.25$ V versus SCE ($\Delta E_2=70$ mV), which are also well-separated from a pseudoreversible two-electron oxidation wave at $E_3=+0.66$ V versus SCE ($\Delta E_3=90$ mV) (solid line in Figure 4c). The mono- or bielectronic nature of each redox process for **1d**–**3d** has been confirmed by rotating-disk electrode (RDE) measurements (dotted lines in Figure 4).

The rich redox behavior for **1d**–**3d** depending on the different nuclearity and the distinct metal coordination environments of each species can be appropriately interpreted

The trend in both the thermodynamic and the kinetic stability of the oxidized, mixed-valent copper(II,III) and high-valent copper(III) species along this series is as expected on the basis of ligand field-stabilization effects. In fact, the relative gain in crystal-field stabilization energy for the change from a square planar d^9 Cu^{II} to a low-spin d^8 Cu^{III} electronic configuration is the main factor in the overall thermodynamic stability of related mononuclear copper(III) complexes with oxamidato and/or oxamato donor groups.[23a] Thus, lower potentials and higher reversibility are associated with the oxidation of the inner Cu^{II} ions with a CuN_4 chromophore (E values in the range of $+0.14$ to 0.25 V vs. SCE and ΔE values of 70 mV) when compared with those of the outer Cu^{II} ions with a CuN_2O_2 chromophore (E values in the range of $+0.43$ to 0.67 V vs. SCE and ΔE values in the range of 80 to 100 mV), as previously reported.[23a] In this case, the stabilization of the trivalent oxidation state of copper is explained in terms of the stronger ligand field afforded by the *N,N′*-oxamidato groups compared to that of the *N,O*-oxamato ones, as evidenced by the visible absorption maxima of the corresponding oligonuclear copper(II) complexes **1d**–**3d** (see the Experimental Section).

Magnetic properties: The $\chi_M T$ versus T plots of **1d**–**3d**, χ_M being the molar magnetic susceptibility per $Cu^{II}{}_n$ ($n=2$–4) unit and T the temperature, are shown in Figure 5. At room temperature, $\chi_M T$ is equal to 0.84 (**1d**), 1.27 (**2d**), and 1.69 $cm^3 mol^{-1} K$ (**3d**), values that are close to those expected for either two, three, or four magnetically noninteracting Cu^{II} ions, respectively [$\chi_M T = n \times (N\beta^2 g_{Cu}{}^2/3k) S_{Cu}(S_{Cu}+1) =$ 0.83 ($n=2$), 1.26 ($n=3$), and 1.69 $cm^3 mol^{-1} K$ ($n=4$) with β is the Bohr magneton, k is the Boltzman constant, g_{Cu} is the Zeeman factor for the Cu^{II} ion, with a value of 2.1, and $S_{Cu}={}^1/_2$]. The value of $\chi_M T$ continuously increases upon cooling to reach maximum $\chi_M T$ values of 1.07 (**1d**), 2.07 (**2d**), and 3.26 $cm^3 mol^{-1} K$ (**3d**) (Figure 5a). This magnetic behavior is characteristic of an overall intramolecular ferromagnetic coupling between the local spin doublets ($S_{Cu}={}^1/_2$) of each Cu^{II} ion to give a resultant high-spin $S = n \times S_{Cu}$ ground state for the $Cu^{II}{}_n$ linear entity. In fact, the maximum $\chi_M T$ values at 6.5 (**1d**) and 2.0 K (**2d** and **3d**) are close to those expected for $S=1$ $Cu^{II}{}_2$, $S={}^3/_2$ $Cu^{II}{}_3$, and $S=2$ $Cu^{II}{}_4$ ground states, respectively ($\chi_M T = (N\beta^2 g^2/3k) S(S+1) = 1.10$ ($n=2$), 2.07 ($n=3$), and 3.31 $cm^3 mol^{-1} K$ ($n=4$) with $g = g_{Cu} = 2.1$ and $S = n \times S_{Cu}$). Upon cooling further, $\chi_M T$ for **1d** slightly decreases, likely due to zero-field splitting (ZFS) effects of the $S=1$ $Cu^{II}{}_2$ ground state (inset of Figure 5a).

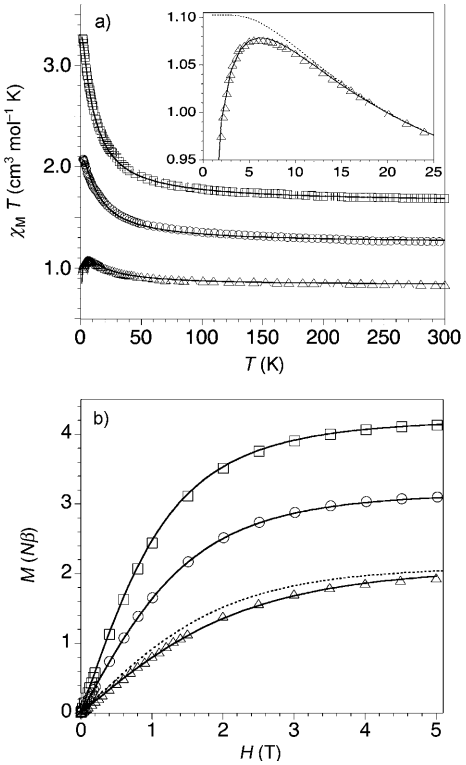

Figure 5. a) $\chi_M T$ versus T and b) M versus H plots at 2.0 K of **1d** (△), **2d** (○), and **3d** (□). The inset shows the $\chi_M T$ versus T plot of **1d** in the low-temperature region. The solid and dotted lines are the best-fit curves (see text).

The overall ferromagnetic behavior for **1d**–**3d** is confirmed by the M versus H plots at 2.0 K, M being the molar magnetization per $Cu^{II}{}_n$ ($n=2$–4) unit and H the applied field (Figure 5b). Thus, the maximum M values at $H=5.0$ T are 1.94 (**1d**), 3.10 (**2d**), and 4.13 $N\beta$ (**3d**), values that are close to the calculated saturation magnetization values for the parallel ('spin-up') alignment of the local spin doublets of each Cu^{II} ion within the $Cu^{II}{}_n$ linear entity ($M_s = n \times g_{Cu} S_{Cu} N\beta = 2.10$ ($n=2$), 3.15 ($n=3$), and 4.20 $N\beta$ ($n=4$) with $g_{Cu}=2.1$ and $S_{Cu}={}^1/_2$). Moreover, the isothermal magnetization curves of **2d** and **3d** are well matched by the Brillouin functions for a quartet ($S={}^3/_2$) and a quintet ($S=2$) spin state, respectively, with $g=2.1$ (solid lines in Figure 5b). The isothermal magnetization curve of **1d** is, however, slightly below the Brillouin function for a triplet ($S=1$) spin state with $g=2.1$, thus indicating the nonnegligible role of the ZFS effects (dotted line in Figure 5b).

The temperature dependence of the magnetic susceptibility data of **1d**–**3d** was analyzed according to the spin Hamiltonian for di- (**1d**), tri- (**2d**), and tetranuclear (**3d**) linear models [Eqs. (1)–(3)] with $S_i = S_{Cu} = {}^1/_2$ for $i = 1-n$ with $n=$ 2–4, respectively:

$$\mathbf{H} = -J\mathbf{S_1}\cdot\mathbf{S_2} + D\mathbf{S_z^2} + g(\mathbf{S_1}+\mathbf{S_2})\beta H \quad (1)$$

$$\mathbf{H} = -J'(\mathbf{S_1}\cdot\mathbf{S_2} + \mathbf{S_2}\cdot\mathbf{S_3}) - j\mathbf{S_1}\cdot\mathbf{S_3} + g(\mathbf{S_1}+\mathbf{S_3})\beta H + g'\mathbf{S_2}\beta H \quad (2)$$

$$\mathbf{H} = -J'(\mathbf{S_1}\cdot\mathbf{S_2} + \mathbf{S_3}\cdot\mathbf{S_4}) - J''(\mathbf{S_2}\cdot\mathbf{S_3}) - j'(\mathbf{S_1}\cdot\mathbf{S_3} + \mathbf{S_2}\cdot\mathbf{S_4}) + g(\mathbf{S_1}+\mathbf{S_4})\beta H + g'(\mathbf{S_2}+\mathbf{S_3})\beta H \quad (3)$$

in which J, J', and J'' are the magnetic coupling parameters that correspond to the outer–outer, inner–outer, and inner–inner pairwise interactions between the next-neighbor Cu^{II} ions, respectively, whereas j and j' are the magnetic coupling

parameters that correspond to the outer–outer and inner–outer pairwise interactions between the next-nearest-neighbor Cu^{II} ions, respectively (solid and dotted lines, respectively, in Scheme 4). In Equations (1)–(3), D is the axial magnetic anisotropy parameter for the ground $S=1$ state of **1d**, whereas g and g' are the Zeeman factors for the outer and inner Cu^{II} ions of **2d** and **3d**, respectively.

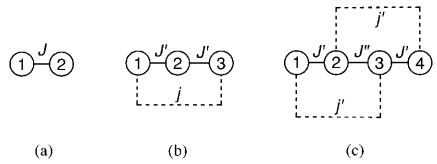

Scheme 4. Spin-coupling model for a) **1d**, b) **2d**, and c) **3d**.

A summary of the least-squares fitting magnetic data through the appropriate analytical expressions [Eqs. (4)–(6)] derived from the above spin Hamiltonians for **1d–3d** is given in Table 7.[26–28] For **2d** and **3d**, the next-nearest-neighbor interactions between the Cu^{II} ions within the Cu^{II}_n ($n=3$ and 4) linear entity were assumed to be negligible (see the theoretical calculations below) and the Zeeman factors of the outer and inner Cu^{II} ions were imposed to be identical [Eqs. (2) and (3) with $j=j'=0$ and $g=g'=g_{Cu}$]. The theoretical curves for **1d–3d** closely follow the experimental data over the whole temperature range (solid lines in Figure 5a). In particular, the theoretical curve for **1d** reproduces well the maximum of $\chi_M T$ that results from the negative axial ZFS of the $S=1$ ground state ($D=1.7\ cm^{-1}$) when compared with that which results by neglecting the axial ZFS ($D=0$), which would exhibit a plateau at low temperatures (solid and dotted lines, respectively, in the inset of Figure 5a). In fact, the isothermal magnetization curve of **1d** is well reproduced by the theoretical curve for a triplet spin state with $g=2.1$ and $D=+1.7\ cm^{-1}$ obtained by the fit of the magnetic susceptibility data (solid line in Figure 5b).

Table 7. Selected magnetic data for **1d–3d**.

Complex	J[a] [cm^{-1}]	J'[a] [cm^{-1}]	J''[a] [cm^{-1}]	D[b] [cm^{-1}]	g_{Cu}[c]	R[d] $\times 10^5$
1d	+16.4			+1.7	2.10	2.5
2d		+16.6			2.10	2.6
3d		+15.0	+16.8		2.10	2.4

[a] Magnetic coupling parameters in Equations (1)–(3) (see text). [b] Axial magnetic anisotropy parameter in Equation (1) (see text). [c] Zeeman factor in Equations (1)–(3) (see text). [d] Agreement factor defined as $R=\Sigma[(\chi_M T)_{exp}-(\chi_M T)_{calcd}]^2/\Sigma[(\chi_M T)_{exp}]^2$.

$$\chi_M T = (2N\beta^2 g_{Cu}{}^2/3k_B)\ [(2T/D)\exp(2D/3kT) + (1-2T/D)\exp(-D/3kT)]/[\exp(2D/3k_BT) + 2\exp(-D/3k_BT) + \exp(-J/k_BT)] \quad (4)$$

$$\chi_M T = (N\beta^2 g_{Cu}{}^2/4k_B)[10 + \exp(-J'/2k_BT) + \exp(-3J'/2k_BT)]/[2 + \exp(-J'/2k_BT) + \exp(-3J'/2k_BT)] \quad (5)$$

$$\chi_M T = (2N\beta^2 g_{Cu}{}^2/k_B)[5 + \exp(-J'/k_BT) + \exp\{-[J' + J'' - (J'^2 + J''^2)^{1/2}]/2k_BT\} + \exp\{-[J' + J'' + (J'^2 + J''^2)^{1/2}]/2k_BT\}]/[5 + 3\exp(-J'/k_BT) + 3\exp\{-[J' + J'' - (J'^2 + J''^2)^{1/2}]/2k_BT)\} + 3\exp\{-[J' + J'' + (J'^2 + J''^2)^{1/2}]/2k_BT\} + \exp\{-[2J' + J'' - (4J'^2 - 2J'J'' + J''^2)^{1/2}]/2k_BT)\} + \exp\{-[2J' + J'' + (4J'^2 - 2J'J'' + J''^2)^{1/2}]/2k_BT\}] \quad (6)$$

The moderate ferromagnetic coupling between the Cu^{II} ions within the Cu^{II}_n ($n=2$–4) linear entity for **1d** ($J=+16.4\ cm^{-1}$), **2d** ($J'=+16.6\ cm^{-1}$), and **3d** ($J'=+15.0\ cm^{-1}$ and $J''=+16.8\ cm^{-1}$) suggests that the EE interaction through the two 2-methyl-substituted 1,3-phenylenediamidate bridges in an *anti* configuration involves a spin-polarization mechanism, as previously found in the parent *syn* dicopper(II) double mesocate with the unsubstituted bridging ligand *N,N'*-1,3-phenylenebis(oxamate) ($J=+16.8\ cm^{-1}$).[25a] In fact, a moderate ferromagnetic coupling has been reported for two related dicopper(II) double mesocates with diverse coordinating-group-substituted *m*-phenylenediamidate bridging ligands in an *anti* configuration, independently of the nature of the donor groups.[14k,l] In general, there is no simple correlation between the magnitude of the ferromagnetic coupling and the structural and electronic factors for these *anti* dicopper(II) complexes that possess an overall twisted coordination geometry of the Cu^{II} ions and a pronounced distortion from orthogonality between the mean metal basal planes and the benzene rings as those observed in **1d**. Yet the J value is remarkably stronger for the dicopper(II) complex with the *N,N'*-1,3-phenylenebis(pyridine-2-carboxamidate) ligand ($J=+21.1\ cm^{-1}$)[14l] than that found with *N,N'*-1,3-phenylenebis(acetylacetonecarboxamidate) ($J=+14.6\ cm^{-1}$),[14k] which is similar to that found for **1d** ($J=+16.4\ cm^{-1}$). It thus appears that the strength of the ferromagnetic coupling along this series of *anti* dicopper(II) double mesocates with *meta*-substituted phenylene spacers may be tuned by the electronic nature of the donor groups of the bridging ligand. In this regard, a relatively stronger ferromagnetic coupling between the inner Cu^{II} ions ($J''=+16.8\ cm^{-1}$) with respect to that between the outer and inner Cu^{II} ions ($J'=+15.0\ cm^{-1}$) is observed for **3d**, in spite of the larger distortion from planarity of the inner metal atoms compared to the outer ones ($\tau=41.2(2)$ and 38.7(2)°, respectively) and the larger deviation from orthogonality of the mean metal basal planes and the benzene rings ($\phi=119.3(5)$ and 108.9(6)°, respectively) (Table 2). This situation may be also explained by electronic factors associated with the greater spin delocalization from the inner Cu^{II} ions (CuN_4 chromophore) toward the *N,N'*-oxamidato donor

groups compared to that of the outer Cu^{II} ions (CuN_2O_2 chromophore) toward the *N,O*-oxamato ones.

Theoretical calculations: DFT energy calculations on **1d**–**3d** show highest-multiplicity, triplet (**1d**), quartet (**2d**), and quintet (**3d**) spin ground states, which are in agreement with the overall ferromagnetic coupling observed experimentally. A summary of the calculated magnetic coupling parameters for **1d**–**3d** determined from the energy levels of the relevant spin states is given in Table 8 (see the computational methods below). The calculated values of the magnetic coupling parameters that correspond to the outer–outer (J), inner–outer (J'), and inner–inner (J'') pairwise interactions between the next-neighbor Cu^{II} ions for **1d** ($J=+15.8\ cm^{-1}$), **2d** ($J'=+16.1\ cm^{-1}$), and **3d** ($J'=+15.2\ cm^{-1}$ and $J''=+16.5\ cm^{-1}$) agree perfectly well with the experimental ones obtained from the fit of the experimental magnetic susceptibility data (Table 7). In particular, the calculated trend as $J'<J''$ found for **3d** follows that observed experimentally, which is in agreement with the larger electron donor capacity of the *N,N'*-oxamidato donor groups relative to that of the *N,O*-oxamato ones. Moreover, the calculated values of the magnetic coupling parameters that correspond to the outer–outer (j) and inner–outer (j') pairwise interactions between the next-nearest-neighbor Cu^{II} ions for **2d** ($j=+0.01\ cm^{-1}$) and **3d** ($j'=-0.01\ cm^{-1}$) are negligible, thereby ensuring the validity of the model used to fit the experimental magnetic susceptibility data.

Table 8. Selected theoretical data for **1d**–**3d**.

Complex	J[a] [cm^{-1}]	J'[a] [cm^{-1}]	J''[a] [cm^{-1}]	j[a] [cm^{-1}]	j'[a] [cm^{-1}]
1d	+15.8				
2d		+16.1		+0.01	
3d		+15.2	+16.5		−0.01

[a] Magnetic coupling parameters in Equations (1)–(3) (see text).

The natural bond orbital (NBO) analysis of the calculated atomic spin densities for the longer member of this series, as an illustrative example, conforms to a spin polarization mechanism for the propagation of the EE interaction between the linear array of metal centers through the π-type orbital pathways of the two oligo-*m*-phenyleneoxalamide bridging ligands. Despite the significant distortion from planarity of the metal atoms in **3d** ($\tau=38.7(2)$ and $41.2(2)°$) (Table 2), the calculated spin-density distribution for the ground-spin quintet configuration of **3d** shows that the orbitals that contain the unpaired electron ('magnetic orbitals') at each Cu^{II} ion are mainly σ-type $d_{x^2-y^2}$(Cu) orbitals. In fact, these orbitals that point toward the Cu–N/O bonds from the oxamato and/or oxamidato donor groups are largely delocalized into the sp^2(N/O) orbitals (Figure 6). They partly overlap with the available π-type orbitals of the 2-methyl-1,3-phenylene spacers, which are mainly made up by the p_z(C) orbitals from the benzene rings with an almost negligible contribution from the p_z(C) orbital from the methyl substituent. This situation leads to the operation of a σ–π interaction (N–C hyperconjugation) within the π-system of the 2-methyl-1,3-phenylenediamidate bridges that involves the sp^2-type orbitals of the nitrogen atoms that are oriented nearly parallel to the p_z-type orbitals of the carbon atoms because of the almost orthogonal disposition of the metal basal plane of each twisted Cu^{II} ion with respect to the mean plane of the benzene rings in **3d** ($\phi=108.9(6)°$) (Table 2).[26]

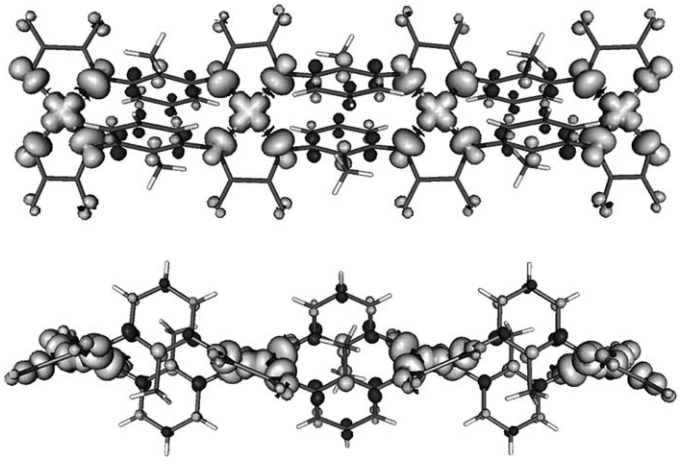

Figure 6. a) Front and b) top projection views of the calculated spin-density distribution for the ground spin quintet configuration of **3d**. Gray and black contours represent positive and negative spin densities, respectively. The isodensity surface corresponds to a value of 0.0025 e $bohr^{-3}$.

The calculated values of the atomic spin density (ρ) along the metal–organic backbone in **3d** provide a precise picture of the relative importance of the spin-delocalization and spin-polarization effects (Scheme 5). Thus, the values of the spin density at the amidate nitrogen donor atoms are large (ρ_N in the range of +0.09 to 0.11 e) and are slightly greater than that at the carboxylate-oxygen ones ($\rho_O=+0.08$ e). More importantly, they have the same sign as those for the copper atoms, which are slightly smaller for the inner than for the outer ones ($\rho_{Cu}=+0.55$ and 0.56 e, respectively). Overall, this situation indicates that the spin delocalization from the metals towards the *N,N'*-oxamidato donor groups dominates over that of the *N,O*-oxamato ones because of the stronger covalency of the Cu–N(amidate) bonds com-

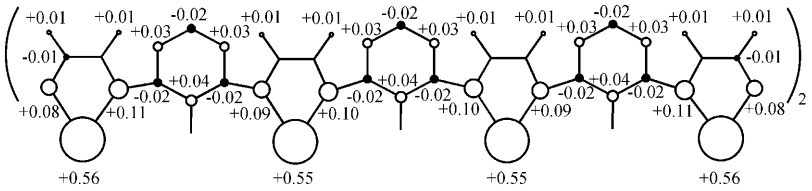

Scheme 5. Spin-density distribution on the metal–organic backbone for **3d** with calculated average atomic spin densities. Empty and full contours represent positive and negative spin densities, respectively.

pared to the Cu–O(carboxylate) ones. On the other hand, the sign alternation of the spin density at the benzene carbon atoms of the 2-methyl-1,3-phenylene spacers agrees with a spin polarization by the amidate nitrogen donor atoms (Scheme 5), thus leading to nonnegligible values of the spin density of the opposite sign at the carbon atoms to which they are directly attached ($\rho_C = -0.02$ e). Because of the *meta*-substitution pattern of the 2-methyl-1,3-phenylene spacers, with an odd number of carbon atoms between the two amidate nitrogen donor atoms, the spin densities at the adjacent copper atoms have identical signs. Hence, a net ferromagnetic exchange interaction results along the linear metal array in **3d**, as expected for the peculiar topology of the oligo-*m*-phenyleneoxalamide bridging ligands.

Conclusion

A novel family of oligonuclear copper(II) string complexes with unique structural and electronic (magnetic and redox) properties have been prepared by following a molecular-programmed approach based on ligand design. In fact, the side-by-side self-assembly of a new generation of linear homo- and heterotopic oligo(2-methyl-1,3-phenyleneoxalamide) ligands by Cu^{II} ions leads to double-stranded, di-, tri-, and tetracopper(II) species of *meso*-helicate type (so-called mesocates) depending on the number of oxalamide metal-binding sites, from two to three and four, respectively. In this case, the unique formation of copper(II) double mesocates is favored because the relatively short and rigid character of the methyl-substituted phenylene spacer prevents the helical twisting of each ligand around the metal centers to give the more common helicates.

These di-, tri-, and tetracopper(II) double mesocates exhibit ferromagnetic and multicenter redox behaviors. Therefore a moderate ferromagnetic coupling between the unpaired electrons of the linearly disposed Cu^{II} ions ($S_{Cu} = {}^1/_2$) through the two 2-methyl-1,3-phenylene spacers of *meta*-substitution pattern is operative along the linear metal array with overall intermetallic distances between the outer metal centers in the range of 0.7–2.2 nm. Moreover, by taking advantage of the distinct electron-donating ability (basicity) of the outer oxamato and the inner oxamidato donor groups, stable mixed-valent tri- and tetracopper(II,III) oxidized species are available through the site-selective oxidation of the inner metal centers. That being so, the ferromagnetic coupling between the unpaired electrons of the outer d^9 Cu^{II} ions ($S_{Cu} = {}^1/_2$) can be interrupted or restored by a reversible redox process that involves the consecutive one-electron oxidation of the inner d^9 Cu^{II} ions ($S_{Cu} = {}^1/_2$) to low-spin d^8 Cu^{III} ions ($S_{Cu} = 0$).

This series of redox-active, ferromagnetically coupled oligonuclear copper(II) double mesocates with high-multiplicity $S = n \times {}^1/_2$ ($n = 2$–4) ground states would thus behave as effective electroswitchable molecular magnetic wires for the transmission of EE interactions of ferromagnetic nature over long distances. In this case, the two *m*-phenylene-type organic spacers act as ferromagnetic coupling units (FCUs) between the outer copper(II)-bis(oxamato) and the inner copper(II)-bis(oxamidato) moieties, which serve in turn as mere spin-containing and redox-switchable spin-containing units, respectively (Scheme 6). In fact, future applications

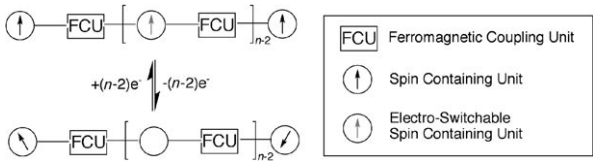

Scheme 6. Spin model of the electroswitchable ferromagnetic coupling in linear oligo-*m*-phenylene oxalamide copper(II) double mesocates.

may be envisaged for this new class of electroswitchable molecular magnetic wires, referred to as 'metal–organic wires' (MOWs), in the emerging field of molecular spintronics as multiple spin-quantum bits (Qubits) and spin-quantum dots.

Experimental Section

Materials: All chemicals were of reagent grade quality and they were purchased from commercial sources and used as received, except those for the electrochemical measurements. The nBu$_4$NPF$_6$ salt was recrystallized twice from ethyl acetate/diethyl ether, dried at 80 °C under vacuum, and kept in an oven at 110 °C. Acetonitrile was purified by distillation from calcium hydride onto activated 3 Å molecular sieves and stored under argon.

Compound $H_2Et_2$1b: Ethyl oxalyl chloride ester (14.0 mL, 120 mmol) was poured into a solution of 2-methyl-1,3-phenylenediamine **1a** (7.32 g, 60 mmol) in THF (250 mL) under vigorous stirring at 0 °C in an ice bath. The reaction mixture was charged with triethylamine (16.8 mL, 120 mmol) and it was heated to reflux for 1 h. The white solid was collected by filtration after cooling, washed thoroughly with water to remove the impurity of Et_3NHCl, and dried under vacuum. Yield: 17.4 g, 90%; ^{1}H NMR (200 MHz, [D$_6$]DMSO, 25 °C, TMS): $\delta = 1.31$ (t, 6H; 2CH$_3$), 2.03 (s, 3H; CH$_3$ of (2-CH$_3$)C$_6$H$_3$), 4.30 (q, 4H; 2CH$_2$O), 7.23 (s, 3H; 4-H, 5-H, and 6-H of (2-CH$_3$)C$_6$H$_3$), 10.42 ppm (s, 2H; 2NH); IR (KBr): $\tilde{\nu} = 3249$ (N–H), 1734, 1683 cm^{-1} (C=O); elemental analysis calcd (%) for C$_{15}$H$_{18}$N$_2$O$_6$: C 55.90, H 5.59, N 8.70; found: C 55.77, H 5.09, N 9.01.

Compound $H_2$2a: Diethyl oxalyl ester (16.0 mL, 80 mmol) was mixed with an excess amount of **1a** (48.8 g, 400 mmol), and the resulting mixture was fused at 120 °C and allowed to react for 24 h under Ar. The gray solid that appeared was collected by filtration, washed thoroughly with methanol to remove the unreacted **1a**, and dried under vacuum. Yield: 17.0 g, 72%; ^{1}H NMR (200 MHz, [D$_6$]DMSO, 25 °C, TMS): $\delta = 2.11$ (s, 6H; 2CH$_3$ of (2-CH$_3$)C$_6$H$_3$), 4.95 (s, 4H; 2NH$_2$), 7.25 (t, 2H; 5-H of (2-CH$_3$)C$_6$H$_3$), 7.35 (d, 4H; 4-H and 6-H of (2-CH$_3$)C$_6$H$_3$), 10.30 ppm (s, 2H; 2NH); IR (KBr): $\tilde{\nu} = 3446$, 3362, 3267 (N–H), 1691, 1621, 1611 cm^{-1} (C=O); elemental analysis calcd (%) for C$_{16}$H$_{18}$N$_4$O$_2$: C 64.43, H 6.04, N 18.7; found: C 65.67, H 5.29, N 19.08.

Compound $H_4Et_2$2b: Ethyl oxalyl chloride ester (7.0 mL, 60 mmol) was poured into a solution of H_2**2a** (8.9 g, 30 mmol) in THF (250 mL) under vigorous stirring at 0 °C in an ice bath. The reaction mixture was charged with triethylamine (8.4 mL, 60 mmol) and it was heated to reflux for 1 h. The white solid was collected by filtration after cooling, washed thoroughly with water to remove the impurity of Et_3NHCl, and dried under vacuum. Yield: 14.4 g, 97%; ^{1}H NMR (200 MHz, [D$_6$]DMSO, 25 °C, TMS): $\delta = 1.32$ (t, 6H; 2CH$_3$), 2.11 (s, 6H; 2CH$_3$ of (2-CH$_3$)C$_6$H$_3$), 4.31

(q, 4H; 2CH_2O), 7.26 (t, 2H; 5-H of (2-CH_3)C_6H_3), 7.37 (d, 4H; 4-H and 6-H of (2-CH_3)C_6H_3), 10.44 ppm (s, 4H; 4NH); IR (KBr): $\tilde{\nu}$ = 3364, 3229 (N−H), 1737, 1687 cm^{-1} (C=O); elemental analysis calcd (%) for $C_{24}H_{26}N_4O_8$: C 57.83, H 5.22, N 11.24; found: C 59.34, H 5.01, N 10.91.

Compound $H_4$3a: H_2Et_2**1b** (6.4 g, 20 mmol) was mixed with an excess amount of **1a** (24.4 g, 200 mmol), and the resulting mixture was fused at 120 °C and allowed to react for 48 h under Ar. The gray solid that appeared was collected by filtration, washed thoroughly with methanol to remove the unreacted **1a**, and dried under vacuum. Yield: 6.4 g, 67%; ^{1}H NMR (200 MHz, [D_6]DMSO, 25 °C, TMS): δ = 2.08 (s, 6H; 2CH_3 of (2-CH_3)C_6H_3), 2.12 (s, 3H; CH_3 of (2-CH_3)C_6H_3), 4.94 (s, 4H; 2NH_2), 7.26 (t, 3H; 5-H of (2-CH_3)C_6H_3), 7.39 (d, 6H; 4-H and 6-H of (2-CH_3)C_6H_3), 10.24 ppm (s, 2H; 4NH); IR (KBr): $\tilde{\nu}$ = 3349, 3254 (N−H), 1711, 1698 cm^{-1} (C=O); elemental analysis calcd (%) for $C_{25}H_{26}N_6O_4$: C 63.29, H 5.49, N 17.72; found: C 63.87, H 5.33, N 18.02.

Compound $H_6Et_2$3b: Ethyl oxalyl chloride ester (2.3 mL, 20 mmol) was poured into a solution of H_4**3a** (4.7 g, 10 mmol) in THF (250 mL) under vigorous stirring at 0 °C in an ice-bath. The reaction mixture was charged with triethylamine (2.8 mL, 20 mmol) and it was heated to reflux for 1 h. The white solid was collected by filtration after cooling, washed thoroughly with water to remove the impurity of Et_3NHCl, and dried under vacuum. Yield: 6.3 g, 93%; ^{1}H NMR (200 MHz, [D_6]DMSO, 25 °C, TMS): δ = 1.32 (t, 6H; 2CH_3), 2.09 (s, 6H; 2CH_3 of (2-CH_3)C_6H_3), 2.14 (s, 3H; CH_3 of (2-CH_3)C_6H_3), 4.31 (q, 4H; 2CH_2O), 7.26 (t, 3H; 5-H of (2-CH_3)C_6H_3), 7.39 (d, 6H; 4-H and 6-H of (2-CH_3)C_6H_3), 10.45 ppm (s, 6H; 6NH); IR (KBr): $\tilde{\nu}$ = 3368, 3265 (N−H), 1696, 1679 cm^{-1} (C=O); elemental analysis calcd (%) for $C_{33}H_{34}N_6O_{10}$: C 58.75, H 5.04, N 12.46; found: C 57.33, H 5.54, N 12.94.

Compound $Na_4[Cu_2(1b)_2]\cdot 6H_2O$ (1c): An aqueous solution (5 mL) of $Cu(NO_3)_2\cdot 3H_2O$ (0.48 g, 2 mmol) was added dropwise to a solution of H_2Et_2**1b** (0.64 g, 2 mmol) and NaOH (0.32 g, 8 mmol) in water (25 mL) under stirring at room temperature. The resulting deep green solution was then filtered, and the solvent was reduced under vacuum until a dark green solid appeared. The solid **1c** was collected by filtration, washed with acetone and diethyl ether, and dried under vacuum. Yield: 0.8 g, 90%; IR (KBr): $\tilde{\nu}$ = 1638, 1613 cm^{-1} (C=O); UV/Vis (H_2O): λ_{max} (ε) = 230 (30800), 300 (7500), 370 (3020), 645 nm (210 $M^{-1}cm^{-1}$); elemental analysis calcd (%) for $C_{22}H_{24}Cu_2Na_4N_4O_{18}$: C 31.03, H 2.84, N 6.58; found: C 30.87, H 2.89, N 6.50.

Compound $(nBu_4N)_4[Cu_2(1b)_2]\cdot 4H_2O$ (1d): A 1.0 M solution of nBu_4NOH in methanol (8.0 mL, 8.0 mmol) was added all at once to an aqueous suspension of H_2Et_2**1b** (0.64 g, 2 mmol) in water (25 mL). An aqueous solution (5 mL) of $CuCl_2\cdot 2H_2O$ (0.34 g, 2 mmol) was then added dropwise under stirring at room temperature to the reaction mixture. The resulting deep green solution was extracted with dichloromethane. The organic phase was separated from the mixture, washed twice with water, and dried over molecular sieves. The solvent was removed under vacuum and the green solid was recuperated with acetone, collected by filtration, and dried under vacuum. Large dark green cubes of **1d** suitable for X-ray diffraction were obtained by recrystallization in acetonitrile after several days of slow evaporation in air at room temperature. Yield: 1.4 g, 85%; IR (KBr): $\tilde{\nu}$ = 1647, 1614 cm^{-1} (C=O); UV/Vis (CH_3CN): λ_{max} (ε) = 230 (28900), 300 (6000), 385 (2150), 600 nm (220 $M^{-1}cm^{-1}$); elemental analysis calcd (%) for $C_{86}H_{164}Cu_2N_8O_{16}$: C 61.00, H 9.76, N 6.62; found: C 61.55, H 9.67, N 6.55.

Compound $Na_6[Cu_3(2b)_2]\cdot 20H_2O$ (2c): An aqueous solution (5 mL) of $Cu(NO_3)_2\cdot 3H_2O$ (0.78 g, 3 mmol) was added dropwise to a solution of H_4Et_2**2b** (1.0 g, 2 mmol) and NaOH (0.48 g, 12 mmol) in water (25 mL) under stirring at room temperature. The resulting deep green solution was then filtered, and the solvent was reduced under vacuum until a dark green solid appeared. The solid **2c** was collected by filtration, washed with acetone and diethyl ether, and dried under vacuum. Yield: 1.4 g, 85%; IR (KBr): $\tilde{\nu}$ = 1654, 1611 cm^{-1} (C=O); UV/Vis (H_2O): λ_{max} (ε) = 240 (51200), 305 (17900), 375 (7180), 588 nm (440 $M^{-1}cm^{-1}$); elemental analysis calcd (%) for $C_{40}H_{64}Cu_3N_8Na_6O_{36}$: C 30.75, H 4.10, N 7.17; found: C 30.15, H 4.00, N 7.04.

Compound $(EtPh_3P)_6[Cu_3(2b)_2]\cdot 26.7H_2O$ (2d): An aqueous solution (10 mL) of $AgNO_3$ (0.50 g, 3 mmol) was added to a solution of **2c** (0.80 g, 0.5 mmol) in water (20 mL) under stirring at room temperature. The dark green solid that appeared was collected by filtration, suspended in water (10 mL), and then charged with a solution of PPh_3EtBr (1.10 g, 3 mmol) in acetonitrile (5 mL). The reaction mixture was further stirred for 30 min under gentle warming and then filtered to remove the precipitate of AgCl. Large dark green cubes of **2d** suitable for X-ray diffraction were obtained by slow evaporation of the filtered solution after several days in air at room temperature. Yield: 1.2 g, 90%; IR (KBr): $\tilde{\nu}$ = 1656, 1612 cm^{-1} (C=O); UV/Vis (CH_3CN): λ_{max} (ε) = 225 (189000), 265 (53000), 390 (3400), 590 nm (405 $M^{-1}cm^{-1}$); elemental analysis calcd (%) for $C_{160}H_{197.4}Cu_3N_8O_{42.7}P_6$: C 58.37, H 6.04, N 3.40; found: C 58.81, H 6.01, N 3.33.

Compound $Na_8[Cu_4(3b)_2]\cdot 16H_2O$ (3c): A solution of $Cu(NO_3)_2\cdot 3H_2O$ (0.96 g, 4 mmol) in DMF (5 mL) was added dropwise to a solution of H_6Et_2**3b** (1.34 g, 2 mmol) and NaH (0.38 g, 16 mmol) in DMF (25 mL) under stirring at room temperature. The deep green solid of **3c** that appeared was collected by filtration, washed with methanol, acetone, and diethyl ether, and dried under vacuum. Yield: 1.8 g, 95%; IR (KBr): $\tilde{\nu}$ = 1625, 1600 cm^{-1} (C=O); UV/Vis (H_2O): λ_{max} (ε) = 245 (77500), 310 (23300), 380 (9980), 593 nm (700 $M^{-1}cm^{-1}$); elemental analysis calcd (%) for $C_{58}H_{68}Cu_4N_{12}Na_8O_{36}$: C 35.77, H 3.49, N 8.63; found: C 35.15, H 3.23, N 8.81.

Compound $(EtPh_3P)_8[Cu_4(3b)_2]\cdot 16H_2O$ (3d): An aqueous solution (10 mL) of $AgNO_3$ (0.66 g, 4 mmol) was added to a solution of **3c** (0.97 g, 0.5 mmol) in water (20 mL) under stirring at room temperature. The dark green solid that appeared was collected by filtration, suspended in water (10 mL), and then charged with a solution of PPh_3EtBr (1.47 g, 4 mmol) in acetonitrile (5 mL). The reaction mixture was further stirred for 30 min under gentle warming and then filtered to remove the precipitate of AgCl. Small dark green cubes of **3d** suitable for X-ray diffraction were obtained by slow evaporation of the filtered solution after several days in air at room temperature. Yield: 1.7 g, 85%; IR (KBr): $\tilde{\nu}$ = 1633, 1602 cm^{-1} (C=O); UV/Vis (CH_3CN): λ_{max} (ε) = 225 (246000), 265 (69500), 400 (8200), 592 nm (735 $M^{-1}cm^{-1}$); elemental analysis calcd (%) for $C_{218}H_{228}Cu_4N_{12}O_{36}P_8$: C 63.95, H 5.61, N 4.11; found: C 63.08, H 5.68, N 4.02.

Physical techniques: Elemental analyses (C, H, N) were performed at the Service Central d'Analyse du CNRS in Vernaison (France). ^{1}H NMR spectra were recorded at room temperature using a Bruker AC 200 (200 MHz) spectrometer. Chemical shifts are reported in δ (ppm) versus TMS with the deuterated DMSO solvent proton residuals as internal standard. FTIR spectra were recorded using Bio-Rad FTS165 spectrophotometers with KBr pellets. UV/Vis solution spectra were recorded at room temperature using an Agilent Technologies 8453 spectrophotometer. Variable-temperature (2.0–300 K) magnetic susceptibility under an applied field of 1 T ($T \geq 25$ K) and 250 G ($T < 25$ K) and variable-field (0–5.0 T) magnetization measurements at T = 2.0 K were carried out on powdered samples of **1d**–**3d** using a SQUID magnetometer. The magnetic susceptibility data were corrected for the diamagnetism of the constituent atoms and the sample holder. Cyclic voltammetry (CV) and rotating-disk electrode (RDE) electrochemical measurements were carried out in acetonitrile using 0.1 M nBu_4NPF_6 as supporting electrolyte and 1.0 mM of **1d**–**3d**. The working electrode in the CV measurements was a glassy carbon disk (0.32 cm^2), which was polished with 1.0 μm diamond powder, washed with absolute ethanol and acetone, and air dried. The reference electrode was $AgClO_4$/Ag separated from the test solution by a salt bridge that contained the solvent/supporting electrolyte, with platinum as auxiliary electrode. All experiments were performed in standard electrochemical cells at 25 °C under argon. The potential range investigated was between −2.0 and 2.0 V versus SCE. The formal potentials were measured at a scan rate of 100 mV s^{-1} and they were referred to the SCE.

Crystal-structure data collection and refinement: The X-ray diffraction data of **1d**–**3d** were collected at 100(2) K with synchrotron radiation (λ = 0.7380 (**1d**) and 0.7513 Å (**2d** and **3d**)) at the BM16-CRG beamline in the ESRF (Grenoble, France). The data for **1d**–**3d** were indexed, integrated, and scaled using the HKL2000 program.[29] All calculations for data reduction, structure solution, and refinement were done by standard procedures (WINGX).[30] The structures of **1d**–**3d** were solved by direct

methods and refined with full-matrix least-squares technique on F^2 using the SHELXS-97 and SHELXL-97 programs.[31] Some disorder was found for one of the two crystallographically independent tetra-*n*-butylammonium cations in **1d**, for which two positions were refined anisotropically using the partition (PART) instruction with occupation factors of 0.648 and 0.352 (equal anisotropic displacement parameter (EADP) instructions were used between identical atoms in the two positions to reduce the number of parameters). In **2d**, residual electronic density was assigned to not-fully-occupied positions for O(13w), O(14w), and O(15w) atoms from crystallization water molecules (site of occupation (s.o.f.) was refined and, once converged, it was fixed to that value for subsequent refinements). The hydrogen atoms from the organic ligands were calculated and refined with isotropic thermal parameters, whereas those from the water molecules were neither found nor calculated. The final geometrical calculations and the graphical manipulations were carried out with PARST97 and CRYSTAL MAKER programs, respectively.[32]

CCDC-777548 (**1d**), 777549 (**2d**), and 777550 (**3d**) contain the supplementary crystallographic data for this paper. These data can be obtained free of charge from The Cambridge Crystallographic Data Centre via www.ccdc.cam.ac.uk/data_request/cif.

Computational methods: The molecular geometries of the model complexes for **1d**–**3d** were not optimized and their bond lengths and interbond angles were taken from the actual crystal structures. The energy for all possible symmetrically independent spin distributions were evaluated. These spin distributions are a high-spin $M_S=1$ and a $M_S=0$ ({1}) state for **1d**, a high-spin $M_S={}^3/_2$ and two $M_S={}^1/_2$ ({1} and {2}) states for **2d**, and a high-spin $M_S=2$, two $M_S=1$ ({1} and {2}), and three $M_S=0$ ({1,2}, ({1,3}, and {1,4}) for **3d** (in this representation, only the center with a spin-down is noted). Electronic structure calculations were carried out with the hybrid density functional B3LYP method[33] combined with the broken-symmetry (BS) approach[34] as implemented in the GAUSSIAN 03 program[35] using the triple-ζ (TZV) quality basis sets proposed by Ahlrichs and co-workers.[36] The electronic density data were obtained using natural bond orbital (NBO) analysis.[37]

Acknowledgements

This work was supported by the MICINN (Spain) (projects CTQ2007-61690, MAT2007-60660, CSD2007-00010, and CSD2006-00015), the Generalitat Valenciana (Spain) (Project PROMETEO/2009/108), the Gobierno Autónomo de Canarias (Spain) (Project PI2002/175), the MESR and the CNRS (France). E.P. acknowledges the MICINN for a postdoctoral ("Juan de la Cierva") grant. J.F.-S. and M.-C. Dul thank the Generalitat Valenciana and the MESR respectively, for predoctoral grants.

[1] a) J. M. Lehn, *Supramolecular Chemistry: Concepts and Perspectives*, VCH, Weinheim, **1995**; b) *Transition Metals in Supramolecular Chemistry, Vol. 5* (Ed.: J. P. Sauvage), Wiley, New York, **1999**.

[2] a) S. Leininger, B. Olenyuk, P. J. Stang, *Chem. Rev.* **2000**, *100*, 853; b) G. F. Swiegers, T. J. Malefetse, *Chem. Rev.* **2000**, *100*, 3483; c) P. J. Steel, *Acc. Chem. Res.* **2005**, *38*, 243.

[3] a) P. J. Stang, B. Olenyuk, *Acc. Chem. Res.* **1997**, *30*, 502; b) S. R. Seidel, P. J. Stang, *Acc. Chem. Res.* **2002**, *35*, 972.

[4] a) M. Albrecht, *Chem. Soc. Rev.* **1998**, *27*, 281; b) M. Albrecht, I. Janser, R. Fröhlich, *Chem. Commun.* **2005**, 157.

[5] a) M. Fujita, *Acc. Chem. Res.* **1999**, *32*, 53; b) M. Fujita, M. Tominaga, A. Hori, B. Therrien, *Acc. Chem. Res.* **2005**, *38*, 369.

[6] a) D. L. Caulder, K. N Raymond, *Acc. Chem. Res.* **1999**, *32*, 975; b) D. Fiedler, D. H. Leung, R. G. Bergman, K. N. Raymond, *Acc. Chem. Res.* **2005**, *38*, 349.

[7] a) R. Ruiz, J. Faus, F. Lloret, M. Julve, Y. Journaux, *Coord. Chem. Rev.* **1999**, *193–195*, 1069; b) E. Pardo, R. Ruiz-García, J. Cano, X. Ottenwaelder, R. Lescouëzec, Y. Journaux, F. Lloret, M. Julve, *Dalton Trans.* **2008**, 2780.

[8] a) L. K. Thompson, *Coord. Chem. Rev.* **2002**, *233–234*, 193; b) L. N. Dawe, T. S. M. Abedin, L. K. Thompson, *Dalton Trans.* **2008**, 1661.

[9] a) J. M. Lehn, *Angew. Chem.* **2004**, *116*, 3728; *Angew. Chem. Int. Ed.* **2004**, *43*, 3644; b) M. Ruben, J. M. Lehn, P. Müller, *Chem. Soc. Rev.* **2006**, *35*, 1056.

[10] a) O. Kahn, *Molecular Magnetism*, VCH, Weinheim, **1993**; b) *Molecular Magnetism: From Molecular Assemblies to the Devices, Vol. 321* (Eds.: E. Coronado, P. Delhaès, D. Gatteschi, J. S. Miller), NATO ASI Ser. E, Kluwer, **1995**; c) *Molecular Electronics* (Eds.: J. Jorner, M. Ratner), Blackwell, Oxford, **1997**; d) *Molecular Electronics: Science and Technology* (Eds.: A. Aviram, M. Ratner), New York Academy of Sciences, New York, **1998**.

[11] a) C. Piguet, G. Bernardinelli, G. Hopfgartner, *Chem. Rev.* **1997**, *97*, 2005; b) M. Albrecht, *Chem. Eur. J.* **2000**, *6*, 3485.

[12] J. M. Lehn, A. Rigault, J. Siegel, J. Harrowfield, B. Chevrier, D. Moras, *Proc. Natl. Acad. Sci. USA* **1987**, *84*, 2565.

[13] a) K. T. Potts, M. K. Keshavarz, F. S. Tham, K. A. G. Raiford, C. Arana, H. D. Abruña, *Inorg. Chem.* **1993**, *32*, 5477; b) L. Zelikovich, J. Libman, A. Shanzer, *Nature* **1995**, *374*, 790; c) P. K. K. Ho, S. M. Peng, K. Y. Wong, C. M. Che, *J. Chem. Soc. Dalton Trans.* **1996**, 1829; d) M. Greenwald, M. Easa, E. Katz, I. Willner, Y. Cohen, *J. Electroanal. Chem.* **1997**, *434*, 77; e) R. W. Saalfrank, A. Dresel, V. Seitz, S. Trummer, F. Hampel, M. Teichert, D. Stalke, C. Stadler, J. Daub, V. Schünemann, A. X. Trautwein, *Chem. Eur. J.* **1997**, *3*, 2058; f) L. J. Charbonnière, A. F. Williams, C. Piguet, G. Bernardelli, E. Rivara-Minten, *Chem. Eur. J.* **1998**, *4*, 485; g) A. El-Ghayouy, A. Harriman, A. De Cian, J. Fischer, R. Ziessel, *J. Am. Chem. Soc.* **1998**, *120*, 9973; h) M. R. Bermejo, M. Fondo, A. M. Gonzales, O. L. Hoyos, A. Sousa, C. A. McAuliffe, W. Hussain, R. Pritchard, V. M. Novotorsev, *J. Chem. Soc. Dalton Trans.* **1999**, 2211; i) K. T. Potts, M. P. Wentland, D. Canguly, G. D. Storrier, S. K. Cha, J. Cha, H. D. Abruña, *Inorg. Chim. Acta* **1999**, *288*, 189.

[14] a) M. Vázquez, M. R. Bermejo, M. Fondo, A. M. González, J. Lahía, L. Sorace, D. Gatteschi, *Eur. J. Inorg. Chem.* **2001**, 1863; b) G. Aromí, P. C. Berzal, P. Gamez, O. Roubeau, H. Kooijman, A. L. Spek, W. L. Driessen, J. Reedijk, *Angew. Chem.* **2001**, *113*, 3552; *Angew. Chem. Int. Ed.* **2001**, *40*, 3444; c) G. Aromí, P. Gamez, O. Roubeau, P. C. Berzal, H. Kooijman, A. L. Spek, W. L. Driessen, J. Reedijk, *Inorg. Chem.* **2002**, *41*, 3673; d) R. Krämer, I. O. Fritsky, H. Pritzkow, L. A. Kovbasyuk, *J. Chem. Soc. Dalton Trans.* **2002**, 1307; e) A. Dei, D. Gatteschi, C. Sangregorio, L. Sorace, M. G. F. Vaz, *Inorg. Chem.* **2003**, *42*, 1701; f) S. Mukherjee, E. Rentschler, T. Weyhermüller, K. Wieghardt, P. Chaudhuri, *Chem. Commun.* **2003**, 1828; g) M. Vázquez, A. Taglietti, D. Gatteschi, L. Sorace, C. Sangregorio, A. M. González, M. Maneiro, R. M. Pedrido, M. R. Bermejo, *Chem. Commun.* **2003**, 1840; h) S. Mukherjee, T. Weyhermüller, E. Bothe, K. Wieghardt, P. Chaudhuri, *Dalton Trans.* **2004**, 3842; i) F. Tuna, M. R. Lees, G. J. Clarkson, M. J. Hannon, *Chem. Eur. J.* **2004**, *10*, 5737; j) A. R. Paital, T. Mitra, D. Ray, W. T. Wong, J. Ribas-Ariño, J. J. Novoa, J. Ribas, G. Aromí, *Chem. Commun.* **2005**, 5172; k) G. Aromi, H. Stoeckli-Evans, S. J. Teat, J. Cano, J. Ribas, *J. Mater. Chem.* **2006**, *16*, 2635; l) M. A. Palacios, A. Rodríguez-Diéguez, A. Sironi, J. M. Herrera, A. J. Mota, J. Cano, E. Colacio, *Dalton Trans.* **2009**, 8538; m) M. A. Palacios, A. Rodríguez-Diéguez, A. Sironi, J. M. Herrera, A. J. Mota, V. Moreno, J. Cano, E. Colacio, *New J. Chem.* **2009**, *33*, 1901; n) L. A. Barrios, D. Aguilà, O. Roubeau, P. Gamez, J. Ribas-Ariño, S. J. Teat, G. Aromi, *Chem. Eur. J.* **2009**, *15*, 11235.

[15] a) J. K. Bera, K. R. Dunbar, *Angew. Chem.* **2002**, *114*, 4633; *Angew. Chem. Int. Ed.* **2002**, *41*, 4453; b) S. Y. Lin, I. W. P. Chen, C. H. Chen, M. H. Hsieh, C. Y. Yeh, T. W. Lin, Y. H. Chen, S. M. Peng, *J. Phys. Chem. B* **2004**, *108*, 959; c) I. P. C. Liu, W. Z. Wang, S. M. Peng, *Dalton Trans.* **2009**, 4323.

[16] a) R. Clérac, F. A. Cotton, L. M. Daniels, K. R. Dunbar, C. A. Murillo, I. Pascual, *Inorg. Chem.* **2000**, *39*, 752; b) J. F. Berry, F. A. Cotton, L. M. Daniels, C. A. Murillo, *J. Am. Chem. Soc.* **2002**, *124*, 3212; c) J. F. Berry, F. A. Cotton, L. M. Daniels, C. A. Murillo, X. Wang, *Inorg. Chem.* **2003**, *42*, 2418; d) J. F. Berry, F. A. Cotton, T. Lu, C. A. Murillo, B. K. Roberts, X. Wang, *J. Am. Chem. Soc.* **2004**,

126, 7082; e) C. K. Kuo, J. C. Chang, C. Y. Yeh, G. H. Lee, C. C. Wang, S. M. Peng, *Dalton Trans.* **2005**, 3696; f) B. Bénard, J. F. Berry, F. A. Cotton, C. Gaudin, X. López, C. A. Murillo, M. M. Rohmer, *Inorg. Chem.* **2006**, *45*, 3932; g) G. C. Huang, M. Bénard, M. M. Rohmer, L. A. Li, M. J. Chiu, C. Y. Yeh, G. H. Lee, S. M. Peng, *Eur. J. Inorg. Chem.* **2008**, 1767; h) F. A. Cotton, C. A. Murillo, Q. Wang, M. D. Young, *Eur. J. Inorg. Chem.* **2008**, 5257; i) X. López, M. M. Rohmer, M. Bénard, *J. Mol. Struct.* **2008**, *890*, 18; j) I. P. C. Liu, C. H. Chen, C. F. Chen, G. H. Lee, S. M. Peng, *Chem. Commun.* **2009**, 577; k) Z. Tabookht, X. López, C. De Graaf, *J. Phys. Chem. B* **2010**, *114*, 2028.

[17] a) F. A. Cotton, L. M. Daniels, C. A. Murillo, X. Wang, *Chem. Commun.* **1998**, 39; b) S. Y. Lai, T. W. Lin, Y. H. Chen, C. C. Wang, G. H. Lee, M. H. Yang, M. K. Leung, S. M. Peng, *J. Am. Chem. Soc.* **1999**, *121*, 250.

[18] a) S. J. Shieh, C. C. Chou, G. H. Lee, C. C. Wang, S. M. Peng, *Angew. Chem.* **1997**, *109*, 57; *Angew. Chem. Int. Ed. Engl.* **1997**, *36*, 56; b) H. C. Chang, J. T. Li, C. C. Wang, T. W. Lin, H. C. Lee, G. H. Lee, S. M. Peng, *Eur. J. Inorg. Chem.* **1999**, 1243; c) C. Y. Yeh, Y. L. Chiang, G. H. Lee, S. M. Peng, *Inorg. Chem.* **2002**, *41*, 4096; d) C. Y. Yeh, C. H. Chou, K. C. Pan, C. C. Wang, G. H. Lee, Y. O. Su, S. M. Peng, *J. Chem. Soc. Dalton Trans.* **2002**, 2670; e) J. F. Berry, F. A. Cotton, P. Lei, T. Lu, C. A. Murillo, *Inorg. Chem.* **2003**, *42*, 3534; f) J. F. Berry, F. A. Cotton, C. S. Fewox, T. Lu, C. A. Murillo, X. Wang, *Dalton Trans.* **2004**, 2297; g) W. Z. Wang, R. H. Ismayilov, R. R. Wang, Y. L. Huang, C. Y. Yeh, G. H. Lee, S. M. Peng, *Dalton Trans.* **2008**, 6808; h) C. X. Yin, J. Su, F. J. Huo, R. H. Ismayilov, W. Z. Wang, G. H. Lee, C. Y. Yeh, S. M. Peng, *J. Coord. Chem.* **2009**, *62*, 2974; i) C. X. Yin, F. J. Huo, W. Z. Wang, R. H. Ismayilov, G. H. Lee, C. Y. Yeh, S. M. Peng, P. Yang, *Chin. J. Chem.* **2009**, *27*, 1295.

[19] a) C. H. Chien, J. C. Chang, C. Y. Yeh, G. H. Lee, J. M. Fang, S. M. Peng, *Dalton Trans.* **2006**, 2106; b) C. H. Chien, J. C. Chang, C. Y. Yeh, J. M. Fang, Y. Song, S. M. Peng, *Dalton Trans.* **2006**, 3249; c) I. P. C. Liu, C. F. Chen, S. A. Hua, C. H. Chen, H. T. Wang, G. H. Lee, S. M. Peng, *Dalton Trans.* **2009**, 3571.

[20] a) Y. H. Chen, C. C. Lee, C. C. Wang, G. H. Lee, S. Y. Lai, S. M. Peng, *Chem. Commun.* **1999**, 1667; b) S. Y. Lai, C. C. Wang, Y. H. Chen, C. C. Lee, Y. H. Liu, S. M. Peng, *J. Chin. Chem. Soc.* **1999**, *46*, 477; c) R. H. Ismayilov, W. Z. Wang, G. H. Lee, C. H. Chien, C. H. Jiang, C. L. Chiu, C. Y. Yeh, S. M. Peng, *Eur. J. Inorg. Chem.* **2009**, 2110.

[21] a) S. M. Peng, C. C. Wang, Y. L. Jang, Y. H. Chen, F. Y. Li, C. Y. Mou, M. K. Leung, *J. Magn. Magn. Mater.* **2000**, *209*, 80; b) R. H. Ismayilov, W. Z. Wang, R. R. Wang, C. Y. Yeh, G. H. Lee, S. M. Peng, *Chem. Commun.* **2007**, 1121; c) R. H. Ismayilov, W. Z. Wang, R. R. Wang, Y. L. Huang, C. Y. Yeh, G. H. Lee, S. M. Peng, *Eur. J. Inorg. Chem.* **2008**, 4290.

[22] a) C. J. Matthews, S. J. Onions, G. Morata, L. J. Davis, S. L. Heath, D. J. Price, *Angew. Chem.* **2003**, *115*, 3274; *Angew. Chem. Int. Ed.* **2003**, *42*, 3166; b) V. Maurizot, G. Linti, I. Huc, *Chem. Commun.* **2004**, 920.

[23] a) R. Ruiz, C. Surville-Barland, A. Aukauloo, E. Anxolabèhere-Mallart, Y. Journaux, J. Cano, M. C. Muñoz, *J. Chem. Soc. Dalton Trans.* **1997**, 745; b) B. Cervera, J. L. Sanz, M. J. Ibañez, G. Vila, F. Lloret, M. Julve, R. Ruiz, X. Ottenwaelder, A. Aukauloo, S. Poussereau, Y. Journaux, M. C. Muñoz, *J. Chem. Soc. Dalton Trans.* **1998**, 781; c) X. Ottenwaelder, R. Ruiz-García, G. Blondin, R. Carrasco, J. Cano, D. Lexa, Y. Journaux, A. Aukauloo, *Chem. Commun.* **2004**, 504; d) X. Ottenwaelder, A. Aukauloo, Y. Journaux, R. Carrasco, J. Cano, B. Cervera, I. Castro, S. Curreli, M. C. Muñoz, A. L. Roselló, B. Soto, R. Ruiz-García, *J. Chem. Soc. Dalton Trans.* **2005**, 2516; e) R. Carrasco, J. Cano, X. Ottenwaelder, A. Aukauloo, Y. Journaux, R. Ruiz-García, *Dalton Trans.* **2005**, 2527.

[24] a) A. Aukauloo, X. Ottenwaelder, R. Ruiz, Y. Journaux, Y. Pei, E. Rivière, B. Cervera, M. C. Muñoz, *Eur. J. Inorg. Chem.* **1999**, 209; b) A. Aukauloo, X. Ottenwaelder, R. Ruiz, S. Poussereau, Y. Pei, Y. Journaux, P. Fleurat, F. Volatron, B. Cervera, M. C. Muñoz, *Eur. J. Inorg. Chem.* **1999**, 1067.

[25] a) I. Fernández, R. Ruiz, J. Faus, M. Julve, F. Lloret, J. Cano, X. Ottenwaelder, Y. Journaux, M. C. Muñoz, *Angew. Chem.* **2001**, *113*, 3129; *Angew. Chem. Int. Ed.* **2001**, *40*, 3039; b) E. Pardo, J. Faus, M. Julve, F. Lloret, M. C. Muñoz, J. Cano, X. Ottenwaelder, Y. Journaux, R. Carrasco, G. Blay, I. Fernández, R. Ruiz-García, *J. Am. Chem. Soc.* **2003**, *125*, 10770; c) E. Pardo, R. Carrasco, R. Ruiz-García, M. Julve, F. Lloret, M. C. Muñoz, Y. Journaux, E. Ruiz, J. Cano, *J. Am. Chem. Soc.* **2008**, *130*, 576; d) M. C. Dul, E. Pardo, R. Lezcouëzec, L. M. Chamoreau, F. Villain, Y. Journaux, R. Ruiz-García, J. Cano, M. Julve, F. Lloret, J. Pasán, C. Ruiz-Pérez, *J. Am. Chem. Soc.* **2009**, *131*, 14614; e) M. C. Dul, X. Ottenwaelder, E. Pardo, R. Lezcouëzec, Y. Journaux, L. M. Chamoreau, R. Ruiz-García, J. Cano, M. Julve, F. Lloret, *Inorg. Chem.* **2009**, *48*, 5244.

[26] a) J. Ferrando-Soria, M. Castellano, C. Yuste, F. Lloret, M. Julve, O. Fabelo, C. Ruiz-Pérez, S.-E. Stiriba, R. Ruiz-García, J. Cano, *Inorg. Chim. Acta* **2010**, *363*, 1666; b) C. Yuste, J. Ferrando-Soria, D. Cangussu, O. Fabelo, C. Ruiz-Pérez, N. Marino, G. De Munno, S.-E. Stiriba, R. Ruiz-García, J. Cano, F. Lloret, M. Julve, *Inorg. Chim. Acta* **2010**, *363*, 1984.

[27] a) Y. Journaux, J. Sletten, O. Kahn, *Inorg. Chem.* **1986**, *25*, 439; b) J. L. Sanz, B. Cervera, R. Ruiz, C. Bois, J. Faus, F. Lloret, M. Julve, *J. Chem. Soc. Dalton Trans.* **1996**, 1359.

[28] a) G. V. Rubenacker, J. E. Drumheller, K. Emerson, R. D. Willet, *J. Magn. Magn. Mater.* **1986**, *54–57*, 1483; b) R. Ruiz, F. Lloret, M. Julve, J. Faus, M. C. Muñoz, X. Solans, *Inorg. Chim. Acta* **1998**, *268*, 263.

[29] Z. Otwinowski, W. Minor, *Processing of X-ray Diffraction Data Collected in Oscillation Mode in Methods in Enzymology: Macromolecular Crystallography, Part A, Vol. 276* (Eds.: C. W. Carter, Jr., R. M. Sweet), Academic Press, New York, **1997**, p. 307.

[30] WINGX: L. J. Farrugia, *J. Appl. Crystallogr.* **1999**, *32*, 837.

[31] SHELX97, Programs for Crystal Structure Analysis, release 97–2, G. M. Sheldrick, Institüt für Anorganische Chemie der Universität Göttingen, Göttingen, **1998**.

[32] a) M. Nardelli, *J. Appl. Crystallogr.* **1995**, *28*, 659; b) CRYSTAL MAKE, D. Palmer, Cambridge University Technical Services, Cambridge, **1996**.

[33] A. D. Becke, *J. Chem. Phys.* **1993**, *98*, 5648.

[34] a) E. Ruiz, J. Cano, S. Alvarez, P. Alemany, *J. Am. Chem. Soc.* **1998**, *120*, 11122; b) E. Ruiz, J. Cano, S. Alvarez, P. Alemany, *J. Comput. Chem.* **1999**, *20*, 1391; c) E. Ruiz, A. Rodriguez-Fortea, J. Cano, S. Alvarez, P. Alemany, *J. Comput. Chem.* **2003**, *24*, 982; d) E. Ruiz, V. Polo, J. Cano, S. Alvarez, *J. Chem. Phys.* **2005**, *123*, 164110.

[35] Gaussian 03, Revision C.02, M. J. Frisch, G. W. Trucks, H. B. Schlegel, G. E. Scuseria, M. A. Robb, J. R. Cheeseman, J. J. A. Montgomery, Jr., T. Vreven, K. N. Kudin, J. C. Burant, J. M. Millam, S. S. Iyengar, J. Tomasi, V. Barone, B. Mennucci, M. Cossi, G. Scalmani, N. Rega, G. A. Petersson, H. Nakatsuji, M. Hada, M. Ehara, K. Toyota, R. Fukuda, J. Hasegawa, M. Ishida, T. Nakajima, Y. Honda, O. Kitao, H. Nakai, M. Klene, X. Li, J. E. Knox, H. P. Hratchian, J. B. Cross, V. Bakken, C. Adamo, J. Jaramillo, R. Gomperts, R. E. Stratmann, O. Yazyev, A. J. Austin, R. Cammi, C. Pomelli, J. W. Ochterski, P. Y. Ayala, K. Morokuma, G. A. Voth, P. Salvador, J. J. Dannenberg, V. G. Zakrzewski, S. Dapprich, A. D. Daniels, M. C. Strain, O. Farkas, D. K. Malick, A. D. Rabuck, K. Raghavachari, J. B. Foresman, J. V. Ortiz, Q. Cui, A. G. Baboul, S. Clifford, J. Cioslowski, B. B. Stefanov, G. Liu, A. Liashenko, P. Piskorz, I. Komaromi, R. L. Martin, D. J. Fox, T. Keith, M. A. Al-Laham, C. Y. Peng, A. Nanayakkara, M. Challacombe, P. M. W. Gill, B. Johnson, W. Chen, M. W. Wong, C. Gonzalez, J. A. Pople, Gaussian, Inc., Wallingford CT, **2004**.

[36] a) A. Schäfer, H. Horn, R. Ahlrichs, *J. Chem. Phys.* **1992**, *97*, 2571; b) A. Schäfer, C. Huber, R. Ahlrichs, *J. Chem. Phys.* **1994**, *100*, 5829.

[37] a) J. E. Carpenter, F. Weinhold, *J. Mol. Struct.* **1988**, *172–191*, 41; b) A. E. Reed, L. A. Curtis, F. Weinhold, *Chem. Rev.* **1988**, *88*, 899; c) F. Weinhold, J. E. Carpenter, *The Structure of Small Molecules and Ions*, Plenum, New York, **1988**, p. 227.

Received: June 18, 2010
Published online: October 22, 2010

